

A Certified Two-Step Port-Reduced Reduced-Basis Component Method for Wave Equation and Time Domain Elastodynamic PDE[☆]

Mohamed Aziz BHOURI^{a,1,*}

^a*Department of Mechanical Engineering, Massachusetts Institute of Technology, 77 Massachusetts Avenue, Cambridge, MA 02139 USA*

Abstract

We present a certified two-step parameterized Model Order Reduction (pMOR) technique for wave equation and elastodynamic Partial Differential Equations (PDE). pMOR techniques for parameterized time domain PDEs offer opportunities for faster solution estimation. However, due to the curse of dimensionality, basic pMOR techniques fail to provide sufficiently accurate approximation when applied for large geometric domains with multiple localized excitations. Moreover, considering the time domain PDE for the construction of the reduced basis greatly increases the computational cost of the offline stage and treatment of hyperbolic PDEs suffers from pessimistic error bounds. Therefore, within the context of linear hyperbolic time domain PDEs for large domains with localized sources, it is of great interest to develop a pMOR approach that provides relatively low-dimensional spaces and which guarantees sufficiently accurate approximations. Towards that end, we develop a two-step Port-Reduced Reduced-Basis Component approach (PR-RBC) for linear hyperbolic time domain PDEs. First, our approach takes advantage of the domain decomposition technique to develop reduced bases for subdomains, which, when assembled, form the domain of interest. This reduces the effective dimensionality of the parameter spaces and solves the curse of dimensionality issue. Moreover, the time domain solution is the inverse Laplace transform of a frequency domain function. Therefore, we can approximate the time domain solution as a linear combination of the PR-RBC solutions to the frequency domain PDE. Hence, we first apply the PR-RBC method on the elliptic frequency domain PDE. Second, we consider the resulting approximations to form a reduced space that is used for the time solver. We also provide an a posteriori error estimate for the two-step PR-RBC approach based on the time-frequency duality.

Keywords: Model order reduction, domain decomposition, parametrized partial differential equations, hyperbolic PDEs, a posteriori error estimate

1. Introduction

Parametric Model Order reduction (pMOR) is a mathematical and computational field of study that aims to reduce the computational cost of the solution to a parameterized mathematical model. pMOR is a subfield to Model Order Reduction (MOR) which is motivated by real-time applications (control, parameter estimation) and many-query applications (design and optimization, uncertainty quantification). Within the real-time application context, the goal is to be able to provide numerical solutions and responses with negligible or no communication with prohibitive offline resources. In many-query applications, the goal is to speed up the computational cost associated with the evaluation of a defined quantity of interest. More specifically, in our work we are interested in the particular pMOR technique employed to approximate a solution to Partial Differential Equation, the Reduced Basis method. The latter consists

[☆]This work was supported by the Office of Naval Research [N00014-17-1-2077]; and the Army Research Office [W911NF1910098]

*Corresponding author

Email address: bhourim@mit.edu (Mohamed Aziz BHOURI)

¹Present address: 3401 Walnut St, Wing A, Office 536, Philadelphia, PA 19104, USA

in constructing one or multiple reduced bases to a high-fidelity approximation to the best-knowledge mathematical model for a particular problem governed by a Partial Differential Equation (PDE). The high-fidelity approximation is generally a discretization scheme such as Finite Element or Finite Volume scheme. In our work we will consider Finite Element method. pMOR approaches intrinsically account for the probabilistic behavior of the parameters governing the system. Therefore, the corresponding numerical model considers the inherent uncertainty in the value of the parameters.

pMOR presents several challenges for applied mathematicians and engineers. Within our context of large domain with localized excitations, the curse of dimensionality is one of the issues that pMOR techniques seek to solve. As a consequence, basic MOR techniques fail to provide sufficiently accurate approximation with relatively low dimensional approximation space for this kind of problem. Moreover, building one or multiple reduced bases to approximate solution to a parametric time domain PDE is generally carried out with considerable computational cost due to the time marching needed within this stage. This is even more hampering for large geometric domains which results in a high-fidelity approximation with a large number of degrees of freedom.

Reduction of time-dependent problems have received a great deal of attention in the reduced-order modeling community. This includes long time integration problems [1] ; Proper Orthogonal Decomposition (POD) based approaches [2, 3, 4] ; Greedy procedure-based methods [5, 6] and hybrid approaches combining POD (in time) and Greedy procedure (in parameter space) [7]. These methods were developed for linear and nonlinear elliptic and parabolic PDEs, and applied to finite element approximations. Reduced basis methods and finite volume discretization of time-dependent PDE have also been developed [8]. However, most of the approaches are based on considering the time as an additional parameter. Therefore, within the offline stage of MOR — in which we build the reduced space — we are required to solve the high-fidelity time-dependent problem for every parameter in the training set, hindering considerably the computational cost of the offline stage. This is even more significant since we generally opt for implicit time integration scheme to ensure stability. In addition, the time-domain elastodynamic PDE is a hyperbolic equation and thus the error estimates developed in the references cited above do not apply. Moreover, RB treatment of hyperbolic equations suffers from pessimistic error bounds [9].

Recent advances in pMOR offer new opportunities for the development of more efficient approaches to approximate linear time domain PDE governing the behavior of systems with large domain and localized excitations. First, frequency-time duality methods speed up computations of reduced bases to linear time domain PDEs, allowing better explorations of the parameter space at a significantly lower computational cost. Second, pMOR techniques which are based on domain decomposition (DD) [10, 11, 12, 13], solve the curse of dimensionality by developing reduced bases for subdomains, which reduces the effective dimensionality of the parameter space considered in the construction of the reduced bases.

To overcome these issues, we develop a two-step PR-RBC method. We use the frequency domain equation (called the Helmholtz equation) obtained by Laplace transform of the time domain equation and consider an augmented parameter set which accounts for the frequency. We apply a Port-Reduced Reduced-Basis Component procedure to approximate the frequency domain equation by developing reduced bases to approximate the solution within archetype components and on boundaries connecting the components. We refer to these boundaries as ports. This corresponds to the first step reduction. Once we consider the global structure formed as an assembly of realizations of the archetype components, we use the PR-RBC bases to compute the global frequency domain solutions at well selected frequencies. Then, we consider these solutions as high-fidelity approximations and use them to form a (final) reduced basis to approximate the global time domain solution. This corresponds to the second step of reduction. In our case we opted for a strong greedy procedure to form the (final) reduced basis that approximates the global time domain solution. Since the time domain solution is the inverse Laplace transform of a frequency domain function that is the solution to the frequency domain equation, we can approximate the time domain solution as a linear combination of the final reduced basis obtained for the frequency domain equation. Hence, we project our time domain equation on the reduced space within which we carry out the time marching using an unconditionally stable scheme. This frequency-time duality is mainly used within the control and dynamics community such as in the elaboration of interpolatory model reduction methods [14, 15]. Nonetheless, a reduced basis method for finite element approximation of time-domain heat equation and wave equation has been developed by taking advantage of the Laplace transform (LT) and inverse LT [16].

A two-step model reduction has been developed previously [17] but is fundamentally different from our approach. Our two-step approach rises from the incorporation of the PR-RBC procedure — applied to the frequency domain

PDE — into the approximation of the time domain PDE. As stated earlier, applying the PR-RBC procedure directly to the time domain PDE will suffer from a prohibitive computation cost in the offline stage to form the PR-RBC reduced bases (offline stage of first step reduction) and from the hyperbolic nature of the time domain PDE, hence the two-step approach solves these two issues. Therefore, we have two model reductions which are completely distinct: the first model reduction consists into the PR-RBC approximation of the frequency domain PDE and the second model reduction consists into building a reduced basis from those PR-RBC approximations — by Proper Orthogonal Decomposition or Greedy procedure — to approximate the time domain PDE by projection it onto the reduced basis obtained. The two-step model reduction developed in [17] relies on an intermediate reduced basis (RB) model of size considerably lower than the high-fidelity approximation — this corresponds to first step of model reduction — and in the second step a derived RB model of dimension lower than the intermediate RB is constructed and considered as the final RB to provide the approximation. Hence, the two model reductions in this contest are not fundamentally distinct as it is the case for our two-step PR-RBC approach to solve the time domain PDE. The method developed in [17] is of great interest in the context of focus calculations — since it permits to considerably reduce the cost of the online stage of MOR when we are interested into a slice or sub-region of a larger parameter domain associated with the intermediate RB model — and in the context of *hp*-RB approximations — since it permits the *hp*-RB treatment of a larger class of problems by a significant reduction in the MOR’s offline stage cost thanks to the replacement of the high-fidelity approximation by the intermediate RB model in the development of the *hp* parameter domain partition. Although the method developed in [17] is a two-step model reduction, it is fundamentally different from the two-step PR-RBC approach developed in this work by the “nature” of the reduction steps that are considered in the two approaches and by the contexts in which each approach is of particular interest.

In case of nonaffine problems that can be introduced for example by the spatial signature of the load on the structure, we recover an approximate affine expansion by means of EQP [18] or EIM [19, 5] to approximate any non-affine dependence on the parameters.

The Port-Reduced, Reduced-Basis Component method [10, 11, 12, 13] provides both very rapid response and also great flexibility in topology and geometry. The two-step PR-RBC, like the simpler classical RB approach, consists of two stages: an offline and an online stage. The offline stage corresponds to the offline stage of first step reduction, while the online stage consists in the online stage of first step reduction, the second step reduction and the time integration. The offline stage of first step reduction may be expensive, however the online stage — which we may invoke many times — is very inexpensive, as it will be shown in the numerical examples.

The two-step PR-RBC approach addresses not a particular “best-knowledge” (bk) model but a family of bk models related through a common physical discipline and hence PDE operator and also typically some unifying engineering context — flexures, airframes, ship loaders, bridges, pipelines, acoustic ducts. Each bk model in our family is characterized by a bk model parameterization, $\{\mu_+, \mathcal{P}_+^{\text{bk}}\}$ (where we lump the frequency into the definition of μ_+ and hence $\mathcal{P}_+^{\text{bk}}$, since we perform the PR-RBC approach on the frequency domain equation). We now describe the offline stage of first step reduction — relevant to our entire family of bk models — and then the online stage of first step reduction — applied to any given bk model in our family.

Offline Stage of First Step Reduction We define a library of parametrized archetype components associated to our family of bk models; we characterize each archetype component by “local” parameters, a reference FE mesh, and local ports for interconnection. This also defines a library of reference ports as the connecting boundary between two archetype components which forms a feasible union via some transformation(s) applied to one or both archetype components. For every archetype component with non-homogeneous Dirichlet boundary condition, we develop a low-dimensional space to approximate the lift function. For every archetype component with inhomogeneity (non-zero source term), we develop a low-dimensional space — Reduced Bubble Space for Inhomogeneity — for the behavior of the solution within the archetype component by a Reduced Basis Weak Greedy approach or POR; we approximate the PDE operator (associated with our family of bk models) in each parametrized archetype component as an affine expansion in (local) parameter. For every reference port, we develop a low-dimensional space — a set of “port modes” — for the behavior of the solution over the reference port by a component-pairwise training procedure. For every port mode, we build a low-dimensional space to approximate the port mode lifting — Reduced Bubble Space for Port-Mode Liftings. We evaluate and store, in an offline dataset, parameter-independent inner products between port modes, bubble modes for inhomogeneity and bubble modes for port mode liftings; in terms of which we may then re-constitute (from our affine expansion) the parameter-dependent PDE bilinear and linear forms.

Online Stage of First Step Reduction: We synthesize any parametrized bk model (in our family of bk models),

for given bk model parameter $\mu_+ \in \mathcal{P}_+^{\text{bk}}$, as an assembly of instantiated archetype components — the value of the local parameter in each instantiated component is determined by the value of the bk model parameter. We connect instantiated components at compatible ports — each pair of local ports coalesces to a single global port Γ in a set G . We map our reduced reference port space to each global port Γ in G to form a reduced global port space and perform static condensation with respect to our global reduced port space — eliminate RB degrees of freedom associated with the Reduced Bubble Space for Inhomogeneity of the instantiated components — to assemble, from the dataset stored in the Offline Stage of First Step Reduction, a reduced Schur complement of size $\sum_{p \in G} M_{\hat{p}} \times \sum_{p \in G} M_{\hat{p}}$, where $M_{\hat{p}}$ is the number of port modes retained for the reference port corresponding to port p . We then solve the Schur complement system for all the port-mode coefficients associated with all the global ports Γ in G . We invoke the Reduced Bubble Space for Port-Mode Liftings to extend the solution field from the ports to the interior of all instantiated components. The global solution is then given by the sum of the reduced basis solutions for inhomogeneity for all components with non-zero source term and/or non-zero Dirichlet boundary condition, and the lifted port modes weighted with the coefficients obtained from the solution to the Schur complement system.

We note that Model Order Reduction plays a central role: port reduction ensures that the Schur complement is small and hence very inexpensive to invert; bubble (and also port) reduction (for Inhomogeneity and for Port-Mode Lifting) ensures that the Schur complement is very inexpensive to form. We emphasize the important role of components. In general, the components divide and conquer the parameter domain: we reduce a large problem with many global parameters, the bk model, to many small problems each with just a few (local) parameters, the instantiated components. Components also permit consideration of very large systems: even in the offline stage of first step reduction we are required to solve FE problems over at most pairs of components — never the full system. And finally, components permit us to more easily justify the pMOR Offline investment in the first step reduction: we may amortize the pMOR Offline effort not only over many queries for any particular bk model, but over all bk models in our family. Note in this sense we can formally define our family of bk models as the set of all models which may be constructed from the associated library of archetype components. This family of bk models can then be well approximated either in the online stage of first step reduction, or in the second step reduction.

Finally, we summarize briefly the parentage of the PR-RBC approach used for the first step reduction. The PR-RBC [10, 20], method is essentially a combination of the Component Model Synthesis (CMS) technique [21, 22, 23] — as regards components and ports — and the Reduced Basis method [24, 25, 26, 19] — as regards bubbles and in particular parametric treatment. The first synthesis of CMS and RB is the Reduced Basis Element method (RBE) [27]; PR-RBC may be viewed as a Reduced Basis Element method for a particular (Static Condensation [28]) choice for the interface treatment and particular strategies for port-mode training [11] and bubble-mode training [29].

An example of the different geometric domains considered in the two-step PR-RBC method is given in figure 1, where components and pairwise components are considered in the offline stage of first step reduction to form the reduced bases, while the structure’s domain is only defined in the online stage of first step reduction (to approximate the solution to the frequency domain PDE) or in the second step reduction (to approximate the solution to the time domain PDE).

The two-step PR-RBC approach is of great interest in the context of Simulation Based Classification (SBC) for Structural Health Monitoring (SHM), which refers to any automated monitoring procedure designed to assess the state of damage of a given aerospace, civil, or mechanical structure of interest. As a model order reduction technique, the two-step PR-RBC method allows the construction of a sufficiently rich and accurate dataset with reasonable computation time, while accounting for the probabilistic nature of the parameters governing our system. Such dataset is used to train classifiers to perform the SBC task. Thanks to the great flexibility in topology and geometry, our two-step PR-RBC method can accommodate for realistic damage instances such as crack existence. In such context, we need to switch in/out damage instances including topological changes which can be carried out efficiently thanks to the two-step PR-RBC method. Our approach also offers flexibility with respect to re-use of components either for variations on a given structure or even for new but similar structures built from the same library of components considered for the two-step PR-RBC method.

Moreover, large deployed mechanical structures, such as offshore platforms and bridges, are subject to ambient-local excitations with probabilistic nuisance parameters. By consequence, harmonic analyses fail to faithfully capture the response of these mechanical structures and time domain characterization is needed. Indeed, modal analyses are typically not very good for local inhomogeneities since eigenfunctions do not well represent local forces whose

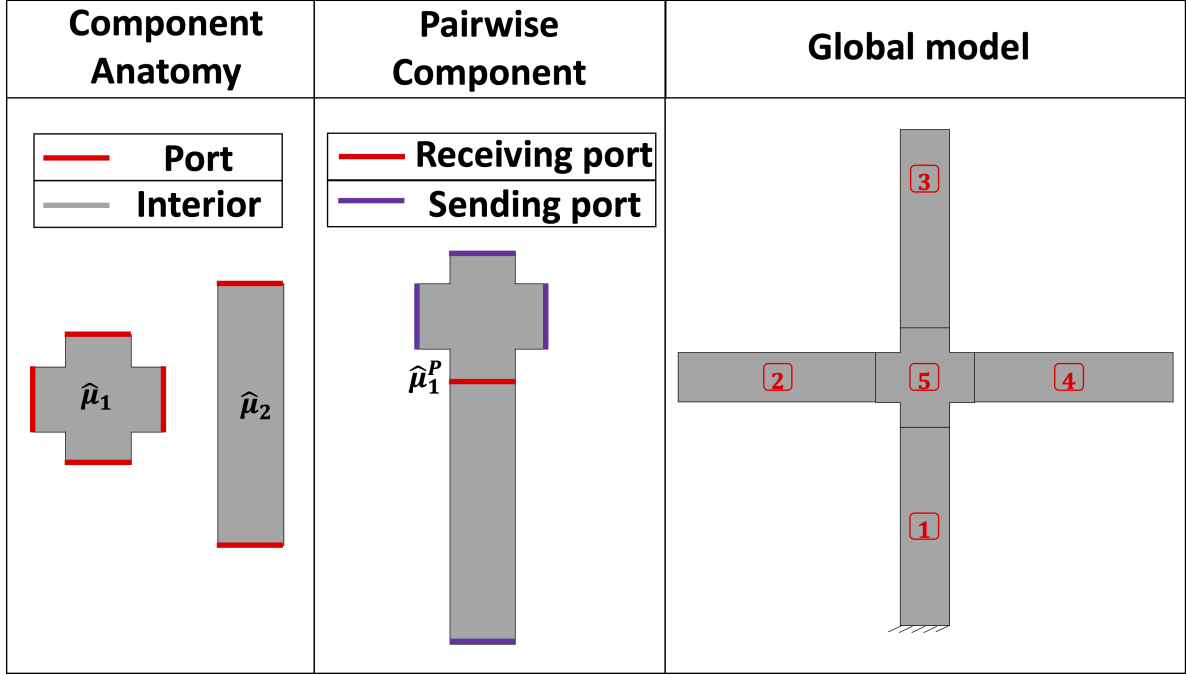


Figure 1: Example of the different geometric domains considered in the two-step PR-RBC method

frequency spectrum is broadly spread over a certain interval. Therefore, for such non-harmonic ambient excitations, we should consider the time domain PDE that governs the behavior of the system and build the corresponding reduced basis using the two-step PR-RBC approach. Second, numerical simulations of large structures are often challenging due to the considerable amount of memory and computation capacity needed, which is more hampering for systems with localized excitations. Such problems involve different scales, and thus numerical methods need to be accurate enough to well approximate the source terms, but also not be computationally prohibitive, which is challenging due to the large geometric domain of the structure. In this context, these forces are applied on regions which are relatively small compared to the size of the global domain and we also need to treat local parameters variation, which is the case for bridges in instance with moving vehicles. Moreover, numerical models should consider the inherent uncertainty in the value of the parameters representing material properties, geometric domains and input forces, which is reflected by the probabilistic nuisance parameters in the SBC task.

Thanks to the domain decomposition procedure and its great flexibility in topology and geometry; the two-step PR-RBC approach solves the above listed challenges and is thus particularly well-suited to SHM. A future work will detail more such implementation.

This work presents the development of an efficient model reduction approach for systems (i) with large geometric domain, (ii) localized excitations, and (iii) governed by hyperbolic linear time domain PDE. Figure 2 provides at a high-level the architecture of the method, and will emphasize on the articulation between the different parts as we give the corresponding details throughout this work.

2. Two-Step Port-Reduced Reduced-Basis Component Method

In this section, we develop a two-step port-reduced reduced-basis component approach (PR-RBC) for linear time-dependent partial differential equations (PDEs). Our field can be either a scalar or a vector. In this section we try to keep the formulation as general as possible. We denote by d_f the dimension of our field, and by d the dimension of the geometrical domain on which we approximate the PDE. The method can be applied for 2-d and 3-d problems. For

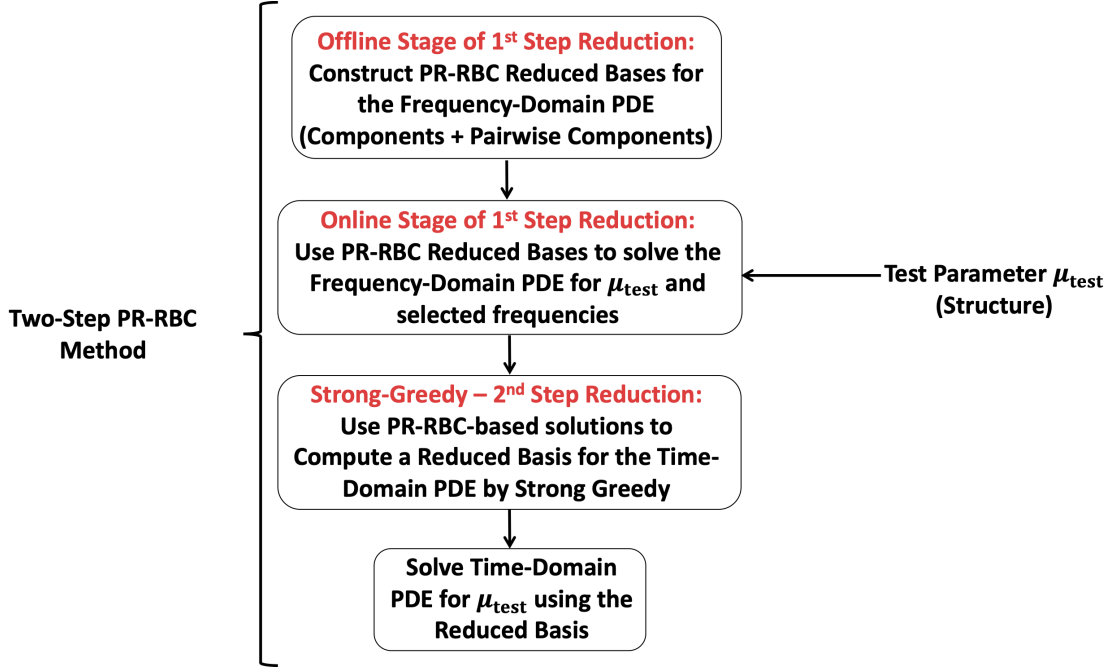


Figure 2: Overall architecture of the two-step PR-RBC method

the numerical experiments of the current work, we restrict ourselves to the 2-d case. Finally, we want to approximate the time domain solution to the PDE over the interval $[0, T_{\text{sim}}]$, for $T_{\text{sim}} > 0$.

For the rest of this work, for two sets of indices \mathcal{E} and \mathcal{E}' , $\mathcal{E} \cup \mathcal{E}'$ refers to

$$\mathcal{E} \cup \mathcal{E}' \equiv \{\mathcal{E}(1), \dots, \mathcal{E}(N^E), \mathcal{E}'(1), \dots, \mathcal{E}'(N^{E'})\}, \quad (1)$$

following this order, where $\mathcal{E} = \{\mathcal{E}(1), \dots, \mathcal{E}(N^E)\}$ and $\mathcal{E}' = \{\mathcal{E}'(1), \dots, \mathcal{E}'(N^{E'})\}$. For a matrix $\underline{\underline{M}}$, $\underline{\underline{M}}(:, \mathcal{E})$ refers to the columns of $\underline{\underline{M}}$ with their indices being equal to $\{\mathcal{E}(1), \dots, \mathcal{E}(N^E)\}$ following this order, while $\underline{\underline{M}}(\mathcal{E}', :)$ refers to the rows of $\underline{\underline{M}}$ with their indices being equal to $\{\mathcal{E}'(1), \dots, \mathcal{E}'(N^{E'})\}$ following this order. Finally, $\underline{\underline{M}}(\mathcal{E}, \mathcal{E}')$ is such that:

$$\underline{\underline{M}}(\mathcal{E}, \mathcal{E}')_{i,j} = \underline{\underline{M}}_{\mathcal{E}(i), \mathcal{E}'(j)}, \quad 1 \leq i \leq N^E, \quad 1 \leq j \leq N^{E'}. \quad (2)$$

2.1. First Step Reduction

Here we give a very brief summary of the online and offline stages of the first step reduction. Since the first step reduction is carried out on the frequency domain equation, the parameter spaces considered for the different archetype components and reference ports correspond the parameter spaces introduced for the time domain PDE augmented with the angular frequency.

We consider a library of \hat{n}_{sub} reference archetype components, each defined by a bounded domain $\hat{\Omega}_i \subset \mathbb{R}^d$, $1 \leq i \leq \hat{n}_{\text{sub}}$ with boundary $\partial\hat{\Omega}_i$. We also introduce our archetype-component-based parameterization $\hat{\mu}_i \in \hat{\mathcal{P}}_i$ for the time domain PDE, where $\hat{\mathcal{P}}_i \in \mathbb{R}^{\hat{n}_i^c}$ is sufficiently large compact set and $\hat{\mu}_i$ follows the probability density function $\hat{\rho}_{\hat{\mu}_i}$ for $1 \leq i \leq \hat{n}_{\text{sub}}$. We note $\hat{\mu}_{+i} = (\hat{\mu}_i, \omega) \in \hat{\mathcal{P}}_+$ the archetype-component-based parameter for the frequency domain

PDE, where ω is the angular frequency and $\hat{\mathcal{P}}_+$ a sufficiently large compact set. For every archetype component i with non-homogeneous Dirichlet boundary conditions, we build a reduced space to approximate the lift functions, and for every archetype component with non-zero source term in the variational formulation, we build a reduced bubble space for inhomogeneity to approximate the non-homogeneous weak form.

We consider a library of \hat{n}_{port} reference ports, each defined from a feasible union of two archetype components via some transformation(s) applied to one or both archetype components. The reference port will be the intersection of the closure of the eventually transformed archetype components. For each feasible union, the archetype components forming such union can be subject to a translation, rotation and dilation to define the reference port. Moreover, for simplicity, we shall presume that ports are mutually disjoint, in which case we may denote the two subdomains associated to a reference port k as $C_{k;1}$ and $C_{k;2}$, such that the reference port is associated to two local ports $\hat{\gamma}_{C_{k;1};j}^P$ and $\hat{\gamma}_{C_{k;2};j'}^P$, which once transformed has to be the same. (We emphasize that the mutually disjoint ports assumption can be relaxed but with some complications).

For every reference port k , we also introduce the domain $\hat{\Omega}_k^P$ formed by the feasible union of the two transformed archetype components. $\partial\hat{\Omega}_k^P$ refers to its boundary and we note $\hat{\Gamma}_k$ as the reference port within the interior of $\hat{\Omega}_k^P$. We also introduce our archetype-port-based parametrization $\hat{\mu}_{+k}^P \in \hat{\mathcal{P}}_{+k}^P$, where $\hat{\mathcal{P}}_{+k}^P \in \mathbb{R}^{\hat{n}_k}$ is sufficiently large compact parameter set that accounts for the angular frequency ω and $\hat{\mu}_{+k}^P$ follows the probability density function $\hat{\rho}_{\hat{\mu}_{+k}^P}^P$, for $1 \leq k \leq \hat{n}_{\text{port}}$. Then for every reference port k , we build a reduce port space by solving a transfer eigenvalue problem such that the reduced space is optimal in the sense of n -Kolmogorov width as shown in [13]. We use a more efficient computational realization of the transfer eigenvalue problem compared to the formalism in [13], since some operations can be simplified analytically. We also build reduced bubble spaces for port-mode liftings.

Referring to the example of the different geometric domains shown in figure 1, the offline stage of first step reduction deals with the construction of reduced bases to approximate the frequency domain PDE within the archetype components and reference ports (defined from the pairwise components forming such ports) as the examples given in the first two plots of figure 1.

Finally, in the context of an offline-online decomposition, we compute and store all the parameter independent bilinear and linear forms evaluation that are needed to solve the reduced basis projected weak forms. We also compute and store the parameter independent bilinear and linear forms evaluation needed to form and solve the Schur complement system. This accounts for different reduced bases constructed for each archetype component: the reduced space to approximate the lift function associated with non-homogeneous Dirichlet boundary condition if any; the reduced bubble space for inhomogeneity associated with non-zero source term if any; the reduced port spaces; and the reduced bubble spaces for port-mode liftings. We opt for a Petrov-Galerkin projection to obtain the reduced Schur complement system, such that our test space is spanned by the non-lifted port-modes (instead of lifted port-modes needed in a Galerkin projection). Such approach is more efficient not only computationally but also in terms of memory storage compared to a Galerkin projection. Moreover, it typically incurs no stability degradation.

2.2. Second Step Reduction: Solution to Time Domain PDE for a Given Model

In this section, we describe the second step reduction to approximate the time domain PDE for a global model. We now consider a given global model characterized by a global parameter $\mu \in \mathcal{P}$ and defined as an assembly of n_{comp} instantiated archetype components to form the global domain Ω . We also define the Hilbert space $X \equiv \{v \in H^1(\Omega) | v|_{\Sigma^D} = 0\}$, where Σ^D is the assumed non-empty part of the boundary on which we impose Dirichlet boundary conditions. We imbue X with inner product $(w, v)_X \equiv \int_{\Omega} \nabla w \cdot \nabla v + wv dV$ and induced norm $\|w\|_X = \sqrt{(w, w)_X}$. We also consider a partitioned $\partial\Omega$ such that $\partial\Omega = \Sigma^D \cup \Sigma^N$, where Σ^N represents the boundary over which we impose Neumann conditions. Each instantiated component c is mapped to an archetype component \mathcal{M}_c^C for which we developed: a reduced bubble space for inhomogeneity in the offline stage of first step reduction if the archetype component has a non-empty inhomogeneous Neumann boundary and/or a reduced basis to approximate the lift function if it has a non-empty inhomogeneous Dirichlet boundary. The value of the local parameter $\mu_{+c}^C \equiv \hat{\mu}_{+\mathcal{M}_c^C}$ for the frequency domain PDE

($\mu_c^C \equiv \hat{\mu}_{\mathcal{M}_c^C}$ for the time domain PDE) in each instantiated component is determined by the value of the global parameter μ_+ for the frequency domain PDE (μ for the time domain PDE respectively). We connect instantiated components at compatible ports such that each pair of local ports coalesces to a single global port p mapped to a reference port \mathcal{M}_p^P for which we developed a reduced port space and reduced bubble spaces for port-mode lifting in the offline stage of first step reduction. The value of the local parameter $\mu_{+p}^P \equiv \hat{\mu}_{+\mathcal{M}_p^P}^P$ for each port is again determined by the value of the global parameter μ_+ . n_{port} refers to the number of global ports. Finally, for the different functions and spaces defined over the archetype components and the reference ports and noted with a hat ($\hat{\cdot}$) in the previous sections, they will be noted without the hat (\cdot) when considering the same functions or spaces but defined over the instantiated components within the global domain Ω . Each instantiated component can be the resultant of a combination of translation, rotation and dilation applied to an archetype component as detailed in previous work [30].

The variational formulation corresponding to the global model reads as follows: Find $u^t(x \in \Omega, t \in [0, T_{\text{sim}}], \mu)$ such that $\forall t \in [0, T_{\text{sim}}], u^t(\cdot, t, \mu) \in X$ and

$$m^t\left(\frac{\partial^2 u^t(\cdot, t, \mu)}{\partial t^2}, v; \mu\right) + c^t\left(\frac{\partial u^t(\cdot, t, \mu)}{\partial t}, v; \mu\right) + a^t(u^t(\cdot, t, \mu), v; \mu) = f^t(v, t; \mu), \quad \forall v \in X, \quad \forall t \in [0, T_{\text{sim}}], \quad (3)$$

$$u^t(x, t, \mu) = 0, \quad \forall x \in \Sigma^D, \quad \forall t \in [0, T_{\text{sim}}] \quad (4)$$

and

$$u^t(t = 0, x, \mu) = u^0(x, \mu); \quad \frac{\partial u^t}{\partial t}(t = 0, x, \mu) = \dot{u}^0(x, \mu), \quad \forall x \in \Omega. \quad (5)$$

Based on (4), we will consider homogeneous Dirichlet boundary conditions. Extension to non-homogeneous Dirichlet boundary conditions can be naturally carried out thanks to the reduced bases that we develop in the offline stage of first step reduction to approximate the lift functions corresponding to such boundary conditions. Indeed, any non-homogeneous Dirichlet boundary condition will simply result in additional terms to consider for the RHS $f^t(\cdot, t; \mu)$ in (3). By applying the Laplace transform to (3) we obtain the Helmholtz equation that we can write as follows, where $u^t(x, t, \mu) = \Re\{u(x, \omega, \mu)e^{i\omega t}\}$:

$$a(u(\cdot, \mu_+), v; \mu_+) = f(v; \mu_+), \quad (6)$$

where $\mu_+ = (\mu, \omega) \in \mathcal{P}_+$ is the augmented parameter to account for the angular frequency ω as we did for the archetype components and reference ports, $a(\cdot, \cdot; \cdot) : H^1(\Omega) \times H^1(\Omega) \times \mathcal{P}_+ \rightarrow \mathbb{R}$ is a bilinear form given by $a(\cdot, \cdot; \cdot) = -\omega^2 \times m^t(\cdot, \cdot; \cdot) + i\omega \times c^t(\cdot, \cdot; \cdot) + a^t(\cdot, \cdot; \cdot)$, $f(\cdot; \cdot) : H^1(\Omega) \times \mathcal{P}_+ \rightarrow \mathbb{R}$ is a linear form that contains the Laplace transform of the $f^t(\cdot, t; \cdot)$ term, as well as the initial conditions terms related to $u^0(x, \mu)$ and $\dot{u}^0(x, \mu)$, and \mathcal{P}_+ refers to the augmented compact parameter set to account for the angular frequency ω . To have an efficient offline-online decomposition for the first stage, we assume an affine parametric dependence of the bilinear and linear forms defined over the archetype components. Such assumption can be recovered by means of EQP or EIM, if needed, and guarantees that the bilinear and linear forms defined over the global model satisfy the same property with respect to μ_+ as follows:

$$a(\cdot, \cdot; \mu_+) = \sum_{r=1}^{Q^{a+}} \Theta_r^{a+}(\mu_+) a_r(\cdot, \cdot); \quad f(\cdot; \mu_+) = \sum_{r=1}^{Q^{f+}} \Theta_r^{f+}(\mu_+) f_r(\cdot). \quad (7)$$

For the first step reduction, we introduce a suitably refined finite element (FE) Galerkin approximation consisting of triangulation $\hat{\mathcal{T}}_i^h$, for each archetype component i . Using those triangulations, we can define the corresponding triangulation obtained for the global domain Ω and associated conforming FE approximation space $X^{Eh} \subset H^1(\Omega)$ of dimension \mathcal{N}^h . For future reference, we provide X^{Eh} with a standard *nodal* basis $\{\varphi_j\}_{j=1, \dots, \mathcal{N}^h}$ and we define $X^h \equiv X \cap X^{Eh}$. We also note $\varphi_{\mathcal{I}(j)}, 1 \leq j \leq \mathcal{N}^{hND}$ the \mathcal{N}^{hND} *nodal* basis functions that are equal to zero over Σ^D and $\varphi_{\mathcal{D}(j)}, 1 \leq j \leq \mathcal{N}^{hD}$ the \mathcal{N}^{hD} *nodal* basis functions that are not identically zero over Σ^D . Then we can define the FE approximation $u^h(x \in \Omega, t \in [0, T_{\text{sim}}], \mu)$ to $u^t(x \in \Omega, t \in [0, T_{\text{sim}}], \mu)$ as follows:

$$\forall t \in [0, T_{\text{sim}}], \quad u^h(\cdot, t, \mu) \in X^h, \quad (8)$$

$$m^t(\frac{\partial^2 u^{th}(\cdot, t, \mu)}{\partial t^2}, v; \mu) + c^t(\frac{\partial u^{th}(\cdot, t, \mu)}{\partial t}, v; \mu) + a^t(u^{th}(\cdot, t, \mu), v; \mu) = f^t(v, t; \mu), \quad \forall v \in X^h, \quad \forall t \in [0, T_{\text{sim}}], \quad (9)$$

$$u^{th}(t = 0, x, \mu) = u^{0h}(x, \mu); \quad \frac{\partial u^{th}}{\partial t}(t = 0, x, \mu) = \dot{u}^{0h}(x, \mu), \quad \forall x \in \Omega, \quad (10)$$

and

$$a(u^h(\cdot, \mu_+), v; \mu_+) = f(v; \mu_+), \quad (11)$$

where $u^{0h}(\cdot, \mu)$ and $\dot{u}^{0h}(x, \mu)$ are respectively the projections of $u^0(\cdot, \mu)$ and $\dot{u}^0(x, \mu)$ on X^h .

To compute a PR-RBC-based approximation, we develop a two-step model order reduction approach. For a test parameter μ^{test} we consider a sufficiently rich set representing the angular frequency ω that we note Ξ_ω of size n_ω and we consider a train dataset $\Xi_{0-t} = \{\mu_+^{\text{test}} \equiv (\mu^{\text{test}}, \omega); \omega \in \Xi_\omega\}$. Note that for the offline stage of first step reduction, we train over a frequency set that at least contains Ξ_ω . Then, we run the online stage of first step reduction for the frequency domain equation for all $\mu_+^{\text{test}} \in \Xi_{0-t}$ which gives n_ω approximations to n_ω frequency domain problems obtained by applying Laplace transform to the time domain variational form (3) - (5). We note such solutions with $u^{h, M', N}(\mu_+^{\text{test}}), \mu_+^{\text{test}} \in \Xi_{0-t}$. This step corresponds to the first model order reduction that we carry out.

For the second model order reduction step, we construct a reduced basis from those approximations by Strong Greedy procedure to identify a reduced space X^{RB} of size N^{RB} , with $\underline{\underline{X}}^{\text{RB}} \in \mathbb{R}^{N^{hND} \times N^{\text{RB}}}$ being the matrix whose columns contain the decomposition of a basis of X^{RB} into $\{\varphi_{I(j)}\}_{1 \leq j \leq N^{hND}}$. Note that in this second model order reduction step, all the time independent parameters are fixed. Hence, only the time dependent parameters and the angular frequency are varying in our parameter step. Therefore, we expect the final reduced space X^{RB} to be of sufficiently small size and also able to provide a sufficient accurate reduced basis approximation to the full FE solution.

We assume that the source term and/or the boundary conditions (such as Neumann or Robin conditions) resulting in the linear form $f^t(v, t; \mu)$, honor a space-time decomposition which can be obtained via some approximation techniques — such as the Empirical Interpolation Method (EIM) — if the original specified boundary condition does not present the decomposition property. Therefore, we have:

$$f^t(\cdot, t; \mu) = \mathcal{F}^t(t, \mu_{\mathcal{F}}^t) \times f^x(\cdot, \overline{\mu_{\mathcal{F}}^t}). \quad (12)$$

where $\mu_{\mathcal{F}}^t$ denotes the parameters governing $\mathcal{F}^t(t, \mu)$, and $\overline{\mu_{\mathcal{F}}^t}$ refers to the rest of them. Since $\mathcal{F}^t(t, \mu_{\mathcal{F}}^t) \rightarrow u^t(\cdot, t, \mu)$ is a linear time invariant system, we can write:

$$u^t(\cdot, t; \mu_{\mathcal{F}}^t, \overline{\mu_{\mathcal{F}}^t}) = \int_{-\infty}^{\infty} \mathcal{F}^t(\tau, \mu) h^t(\cdot, t - \tau; \overline{\mu_{\mathcal{F}}^t}) d\tau, \quad (13)$$

$$u(\cdot, \omega; \mu_{\mathcal{F}}^t, \overline{\mu_{\mathcal{F}}^t}) = h(\cdot, \omega; \overline{\mu_{\mathcal{F}}^t}) \times \mathcal{F}(\omega; \mu_{\mathcal{F}}^t), \quad (14)$$

where $\mathcal{F}(\omega; \mu_{\mathcal{F}}^t) = \mathcal{LT}[\mathcal{F}^t(\cdot, \mu_{\mathcal{F}}^t)]$ (\mathcal{LT} refers to the Laplace transform operator) and $h^t(\cdot, \cdot; \overline{\mu_{\mathcal{F}}^t})$, and $h(\cdot, \cdot; \overline{\mu_{\mathcal{F}}^t})$ denote the time domain and frequency domain representations of the transfer function respectively. If $\mathcal{F}(\omega; \mu_{\mathcal{F}}^t) = 1$, then $u(\cdot, \omega; \mu_{\mathcal{F}}^t, \overline{\mu_{\mathcal{F}}^t}) = h(\cdot, \omega; \overline{\mu_{\mathcal{F}}^t})$. Therefore, if we take $\mathcal{F}(\omega; \mu_{\mathcal{F}}^t) = 1$, then the two-step PR-RBC reduction will learn $h(\cdot, \omega; \overline{\mu_{\mathcal{F}}^t})$ and thus we can well approximate $u(\cdot, \omega; \mu_{\mathcal{F}}^t, \overline{\mu_{\mathcal{F}}^t}) = h(\cdot, \omega; \overline{\mu_{\mathcal{F}}^t}) \times \mathcal{F}(\omega; \mu_{\mathcal{F}}^t)$, $\forall \mathcal{F}(\omega; \mu_{\mathcal{F}}^t)$. Since $u^t(\cdot, t; \mu_{\mathcal{F}}^t, \overline{\mu_{\mathcal{F}}^t}) = \mathcal{LT}^{-1}[u(\cdot, \omega; \mu_{\mathcal{F}}^t, \overline{\mu_{\mathcal{F}}^t})]$, we can also well approximate $u^t(\cdot, t; \mu_{\mathcal{F}}^t, \overline{\mu_{\mathcal{F}}^t})$. For the numerical examples shown in section 2.5, we always consider $\mathcal{F}(\omega; \mu_{\mathcal{F}}^t) = 1$ in the training process to form the two-step PR-RBC reduced bases, and the exact time signature of the load is only used in the time marching performed using the reduced space X^{RB} .

We note the frequency domain matrices $\underline{\underline{\mathcal{A}}}_r^h \in \mathbb{R}^{N^h \times N^h}$ for $1 \leq r \leq Q^{a+}$, the norm matrix $\underline{\underline{X}}^{h, \text{norm}} \in \mathbb{R}^{N^h \times N^h}$, and the vectors $\underline{\underline{\mathcal{F}}}_r^h \in \mathbb{R}^{N^h}$ for $1 \leq r \leq Q^{f+}$, which are defined as:

$$(\underline{\underline{\mathcal{A}}}_r^h)_{qq'} \equiv a_r(\varphi_{q'}, \varphi_q), \quad 1 \leq q, q' \leq N^h, \quad (15)$$

$$\left(\underline{\underline{X}}^{h,\text{norm}}\right)_{qq'} \equiv (\varphi_{q'}, \varphi_q)_{H^1(\Omega)}, 1 \leq q, q' \leq N^h \quad (16)$$

and

$$\left(\underline{\underline{\mathcal{F}}}^h\right)_q \equiv f_r(\varphi_q), 1 \leq q \leq N^h. \quad (17)$$

The second step reduction based on Strong Greedy approach is given in Algorithm 1 in Appendix A. For this reduction, we need to estimate the actual error between the high-fidelity solution and the reduced basis one. Therefore, we first need to estimate $\{u^{h,\mathbf{M}',\mathbf{N}}(\cdot; \mu_{+j}^{\text{test}}), \mu_{+j}^{\text{test}} \in \Xi_{0-t}\}$, where Ξ_{0-t} denotes the training set used for the Strong Greedy algorithm, which is done in step 21 of Algorithm 1. Then, at the i -th iteration of the Strong Greedy algorithm — prior to which we have constructed a reduced basis X_i^{RB} of size i — we look for the next snapshot to add to the reduced basis X_i^{RB} among the PR-RBC solutions $\{u^{h,\mathbf{M}',\mathbf{N}}(\cdot; \mu_{+j}^{\text{test}}), \mu_{+j}^{\text{test}} \in \Xi_{0-t}\}$ based on the norm of the error. Since we consider our PR-RBC approximations as high-fidelity solutions within the weak greedy algorithm, the error computed on the RB solution $u^{\text{RB},i}(\mu_+) \in X_i^{\text{RB}}$ is simply given by $\|u^{h,\mathbf{M}',\mathbf{N}}(\cdot; \mu_+) - u^{\text{RB},i}(\mu_+)\|_{H^1(\Omega)}$. Therefore, at the i -th iteration of the Weak Greedy algorithm, we compute $\|u^{h,\mathbf{M}',\mathbf{N}}(\cdot; \mu_{+j}^{\text{test}}) - u^{\text{RB},i}(\mu_{+j}^{\text{test}})\|_{H^1(\Omega)}$ for $\mu_{+j}^{\text{test}} \in \Xi_{0-t}$. An efficient computation of these quantities is detailed in Algorithm 1 and the final affectation to compute $\|u^{h,\mathbf{M}',\mathbf{N}}(\cdot; \mu_{+j}^{\text{test}}) - u^{\text{RB},i}(\mu_{+j}^{\text{test}})\|_{H^1(\Omega)}$ is done in step 50 of Algorithm 1. We then note $\mu_{+i}^{\text{test}*} \in \Xi_{0-t}$ such that $\|u^{h,\mathbf{M}',\mathbf{N}}(\cdot; \mu_{+i}^{\text{test}*}) - u^{\text{RB},i}(\mu_{+i}^{\text{test}*})\|_{H^1(\Omega)} = \max_{\mu_{+j}^{\text{test}} \in \Xi_{0-t}} \|u^{h,\mathbf{M}',\mathbf{N}}(\cdot; \mu_{+j}^{\text{test}}) - u^{\text{RB},i}(\mu_{+j}^{\text{test}})\|_{H^1(\Omega)}$. This is done in step 52 of Algorithm

1. We consider the normalized error defined as:

$$e(\mu_{+i}^{\text{test}*}) \equiv \frac{\|u^{h,\mathbf{M}',\mathbf{N}}(\cdot; \mu_{+i}^{\text{test}*}) - u^{\text{RB},i}(\mu_{+i}^{\text{test}*})\|_{H^1(\Omega)}}{\|u^{h,\mathbf{M}',\mathbf{N}}(\cdot; \mu_{+1}^{\text{test}*}) - u^{\text{RB},1}(\mu_{+1}^{\text{test}*})\|_{H^1(\Omega)}} = \frac{\max_{\mu_{+j}^{\text{test}} \in \Xi_{0-t}} \|u^{h,\mathbf{M}',\mathbf{N}}(\cdot; \mu_{+j}^{\text{test}}) - u^{\text{RB},i}(\mu_{+j}^{\text{test}})\|_{H^1(\Omega)}}{\max_{\mu_{+j}^{\text{test}} \in \Xi_{0-t}} \|u^{h,\mathbf{M}',\mathbf{N}}(\cdot; \mu_{+j}^{\text{test}}) - u^{\text{RB},1}(\mu_{+j}^{\text{test}})\|_{H^1(\Omega)}}, \quad (18)$$

as an error indicator for convergence, which is done in step 53 of Algorithm 1. If the normalized error is larger than a certain threshold ϵ given as an input to Algorithm 1, then we extend X_i^{RB} as $X_{i+1}^{\text{RB}} \leftarrow X_i^{\text{RB}} \oplus u^{h,\mathbf{M}',\mathbf{N}}(\cdot; \mu_{+i}^{\text{test}*})$ provided that $i+1$ is less than the size of the training set Ξ_{0-t} and that $i < N$ for a certain threshold N specified as an input. Otherwise, the final reduced space X^{RB} is simply given by X_i^{RB} .

In step 21 of Algorithm 1, we call the first step reduction's online stage algorithm (noted PR-RBC-1st-step-reduction-Online) to compute the PR-RBC approximation to the frequency domain equation with the parameter $(\mu^{\text{test}}, \omega_i)$.

The affine parametric dependence of the time domain bilinear and linear forms can be written as follows:

$$\hat{m}^t(\cdot, \cdot; \mu) = \sum_{r=1}^{Q^m} \Theta_r^m(\mu) m_r^t(\cdot, \cdot); a^t(\cdot, \cdot; \mu) = \sum_{r=1}^{Q^a} \Theta_r^a(\mu) a_r^t(\cdot, \cdot); c^t(\cdot, \cdot; \mu) = \sum_{r=1}^{Q^c} \Theta_r^c(\mu) c_r^t(\cdot, \cdot) \quad (19)$$

and

$$f^t(\cdot, t; \mu) = \mathcal{F}_\mu^t(t, \mu) \times \sum_{r=1}^{Q^f} \Theta_r^f(\mu) f_r^t(\cdot). \quad (20)$$

We note the time domain matrices $\underline{\underline{\mathcal{A}}}^{th} \in \mathbb{R}^{N^h \times N^h}$ for $1 \leq r \leq Q^a$, $\underline{\underline{\mathcal{C}}}^{th} \in \mathbb{R}^{N^h \times N^h}$ for $1 \leq r \leq Q^c$, $\underline{\underline{\mathcal{M}}}^{th} \in \mathbb{R}^{N^h \times N^h}$ for $1 \leq r \leq Q^m$ and vectors $\underline{\underline{\mathcal{F}}}^{th} \in \mathbb{R}^{N^h}$ for $1 \leq r \leq Q^f$, which are defined as:

$$\left(\underline{\underline{\mathcal{A}}}^{th}\right)_{qq'} \equiv a_r^t(\varphi_{q'}, \varphi_q), 1 \leq q, q' \leq N^h, \quad (21)$$

$$\left(\underline{\underline{\mathcal{C}}}^{th}\right)_{qq'} \equiv c_r^t(\varphi_{q'}, \varphi_q), 1 \leq q, q' \leq N^h, \quad (22)$$

$$\left(\underline{\underline{\mathcal{M}}}^{th}\right)_{qq'} \equiv m_r^t(\varphi_{q'}, \varphi_q), 1 \leq q, q' \leq N^h, \quad (23)$$

and

$$(\underline{\mathcal{F}}_r^{th})_q \equiv f_r^t(\varphi_q), 1 \leq q \leq N^h. \quad (24)$$

We then evaluate the following matrices and vectors:

$$\underline{\underline{\mathcal{M}}}_{\mu^{\text{test}}}^{th} = \sum_{r=1}^{Q^m} \Theta_r^m(\mu^{\text{test}}) \underline{\underline{\mathcal{M}}}_r^{th}, \quad (25)$$

$$\underline{\underline{\mathcal{C}}}_{\mu^{\text{test}}}^{th} = \sum_{r=1}^{Q^c} \Theta_r^c(\mu^{\text{test}}) \underline{\underline{\mathcal{C}}}_r^{th}, \quad (26)$$

$$\underline{\underline{\mathcal{A}}}_{\mu^{\text{test}}}^{th} = \sum_{r=1}^{Q^a} \Theta_r^a(\mu^{\text{test}}) \underline{\underline{\mathcal{A}}}_r^{th} \quad (27)$$

and

$$\underline{\underline{\mathcal{F}}}_{\mu^{\text{test}}}^{th} = \sum_{r=1}^{Q^f} \Theta_r^f(\mu^{\text{test}}) \underline{\underline{\mathcal{F}}}_r^{th}, \quad (28)$$

and the reduced basis-based ones:

$$\underline{\underline{\mathcal{M}}}_{\mu^{\text{test}}}^{\text{tRB}} = (\underline{\underline{\mathcal{X}}}^{\text{BR}})^\dagger \times \underline{\underline{\mathcal{M}}}_{\mu^{\text{test}}}^{th} (I(:, I(:))) \times \underline{\underline{\mathcal{X}}}^{\text{BR}}, \quad (29)$$

$$\underline{\underline{\mathcal{C}}}_{\mu^{\text{test}}}^{\text{tRB}} = (\underline{\underline{\mathcal{X}}}^{\text{BR}})^\dagger \times \underline{\underline{\mathcal{C}}}_{\mu^{\text{test}}}^{th} (I(:, I(:))) \times \underline{\underline{\mathcal{X}}}^{\text{BR}}, \quad (30)$$

$$\underline{\underline{\mathcal{A}}}_{\mu^{\text{test}}}^{\text{tRB}} = (\underline{\underline{\mathcal{X}}}^{\text{BR}})^\dagger \times \underline{\underline{\mathcal{A}}}_{\mu^{\text{test}}}^{th} (I(:, I(:))) \times \underline{\underline{\mathcal{X}}}^{\text{BR}}, \quad (31)$$

and

$$\underline{\underline{\mathcal{F}}}_{\mu^{\text{test}}}^{\text{tRB}} = (\underline{\underline{\mathcal{X}}}^{\text{BR}})^\dagger \times \underline{\underline{\mathcal{F}}}_{\mu^{\text{test}}}^{th} (I(:)). \quad (32)$$

Then we introduce a finite-difference discretization scheme in time. We fix N_t the number of time steps and define $\Delta t = T_{\text{sim}}/N_t$; $t_j \equiv j\Delta t$, $0 \leq j \leq N_t$. Note that our method can be applied to any finite-difference scheme. We just opt for a particular one in this work for sake of clarity. We choose the Newmark- β scheme with $\beta_t = \frac{1}{4}$ and $\gamma_t = \frac{1}{2}$ such that it is unconditionally stable, since we have the following properties [31, 32]:

$\gamma_t < \frac{1}{2}$: unstable.

$\gamma_t \leq 2\beta_t \leq 1$: unconditionally stable.

$0 \leq 2\beta_t < \gamma_t$: CFL condition.

We also consider the following time marching matrix:

$$\underline{\underline{\mathcal{T}}}_{\mu^{\text{test}}}^{\text{RB}} = \underline{\underline{\mathcal{M}}}_{\mu^{\text{test}}}^{\text{RB}} + \Delta t \times \gamma_t \times \underline{\underline{\mathcal{C}}}_{\mu^{\text{test}}}^{\text{RB}} + \Delta t^2 \times \beta_t \times \underline{\underline{\mathcal{A}}}_{\mu^{\text{test}}}^{\text{RB}}. \quad (33)$$

Finally, if we note $\underline{\underline{\mathcal{U}}}_0^h \in \mathbb{R}^{N^{hND}}$ and $\underline{\underline{\mathcal{U}}}_0^h \in \mathbb{R}^{N^{hND}}$ the FE evaluation vectors of the initial conditions $u^0(\cdot, \mu^{\text{test}})$ and $\dot{u}^0(\cdot, \mu^{\text{test}})$, then the online stage of two-step reduction's algorithm is detailed in Algorithm 2 in Appendix A, in which we perform the time marching and obtain $\{\underline{\underline{\mathcal{U}}}_j^{\text{RB}}(\mu^{\text{test}})\}_{1 \leq j \leq N_t}$ as output.

The reduced basis approximation of $u^{th}(\cdot, \cdot, \mu^{\text{test}})$ at the time integration step t_j is then given by:

$$u^{\text{tRB}}(\cdot, t_j, \mu^{\text{test}}) = \sum_{j=1}^{N^{hND}} \left(\Re[\underline{\underline{\mathcal{X}}}^{\text{RB}} \times \underline{\underline{\mathcal{U}}}_j^{\text{RB}}(\mu^{\text{test}})] \right)_j \varphi_{I(j)}. \quad (34)$$

We also investigated other alternatives for the second step reduction using Weak Greedy approach or POD instead of the Strong Greedy approach. Greedy approaches are computationally more efficient than POD. For the Weak Greedy method, at the i -th iteration — prior to which we have constructed a reduced basis X_i^{RB} of size i — we look for the next snapshot to add to the reduced basis X_i^{RB} among the PR-RBC solutions $\{u^{h,M',N}(\cdot; \mu_{+j}^{\text{test}}), \mu_{+j}^{\text{test}} \in \Xi_{0-1}\}$ based on the norm of the residual, instead of the actual error used in the Strong Greedy based method that we detailed above. As we did in the Strong Greedy approach, we also consider our PR-RBC approximations as high-fidelity solutions within the weak greedy algorithm. The Weak Greedy approach requires the computation of the residual in the process of building the reduced basis, which involves a matrix inversion, of dimension $\mathcal{N}^{hND} \times \mathcal{N}^{hND}$ in our case. To reduce this computational cost, we took advantage of a Cholesky decomposition. However, such approach would suffer from computational instability for 3D problems. Unlike the Strong Greedy approach, the Weak Greedy based method does not require the estimation of the PR-RBC approximation to the frequency domain equation for all $\omega \in \Xi_\omega$, and thanks to the sparsity of the FE based matrices, the computation costs of lower matrix inversion (to estimate the residual) and of matrix multiplication (to estimate the actual error) are of the same order of magnitude. By consequence, the computational cost of the Weak Greedy based method is slightly lower than the Strong Greedy based one. However, the efficiency of the PR-RBC method considerably reduces the computational cost associated with the PR-RBC approximation to the frequency domain equation and for the stability reason mentioned earlier regarding 3D problems, the Strong Greedy based method is more appropriate than the weak Greedy based approach. These points justify our choice for the Strong Greedy approach, which is the only method that we detail in this work for sake of clarity and conciseness.

2.3. Operation Count

The operation count to estimate $u^{\text{RB}}(\cdot, \cdot, \mu^{\text{test}})$ for $n^{\text{t-t}}$ different parameters μ^{test} using SG-2nd-step-reduction algorithm (Algorithm 1) is equal to:

$$n^{\text{t-t}} \times n_\omega \cdot \left[\sum_{i=1}^{n_{\text{comp}}} (N_i^{\text{inhom}})^3 + \sum_{k=1}^{n_{\text{port}}} \sum_{m=1}^{M'_k} \sum_{\ell=1}^2 (N_{k,m,\ell})^3 + \left(\sum_{k=1}^{n_{\text{port}}} M'_k \right)^\kappa \right] + n^{\text{t-t}} \times n_\omega \cdot \left[(\mathcal{N}^{\text{RB}})^4 + \mathcal{N}^{\text{RB}} \cdot (\mathcal{N}^{hND})^{\kappa'} \right] + n^{\text{t-t}} \times N_t \cdot [(\mathcal{N}^{\text{RB}})^3 + n_{\text{outputs}} \cdot \mathcal{N}^{\text{RB}}] \quad (35)$$

FLOPs, where:

- N_i^{inhom} is the size of the reduced bubble space for inhomogeneity for component i ,
- M'_k the size of reduced port space for port k ,
- $N_{k,m,\ell}$, $\ell = 1, 2$ the size of reduced bubble spaces for port-mode liftings for port k and port mode m within the two components forming the port k ,
- κ a solver-dependent scaling exponent for sparse matrix inversion,
- κ' a solver-dependent scaling exponent for sparse matrix multiplication,
- and n_{outputs} refers to the number of output quantities we are interested in.

The first line of the operation count given in (35) corresponds to calling the online stage of first step reduction n_ω times, while the first term of the second line corresponds to performing the Strong Greedy algorithm and the second one to the time marching using the reduced space X^{RB} .

Computing the FE approximations $u^{th}(\cdot, \cdot, \mu^{\text{test}})$ for $n^{\text{t-t}}$ different parameters μ^{test} would have required:

$$n^{\text{t-t}} \times N_t \cdot ((\mathcal{N}^{hND})^\kappa + n_{\text{outputs}} \cdot \mathcal{N}^{hND}) \quad (36)$$

FLOPs.

Note that in our context of many query, the product $n^{\text{t-t}} \times N_t$ is the largest number within the different terms that we have, hence we expect of course the two-step PR-RBC procedure to have considerably smaller computation cost

compared to the full FE approximation as we will show in the numerical experiments in section 2.5. We note also that the solver scaling exponent κ' is smaller than κ since κ' is related to the computation cost of sparse matrices multiplication, while κ refers to the solver scaling exponent for sparse matrices inversion. In our two-step PR-RBC approach based on Strong Greedy algorithm, we do not have any full FE matrix inversion, thus the term $(\mathcal{N}^{hND})^\kappa$ does not appear in its operation count.

In our context of many query application we compare the cost of the offline stage of the first step reduction plus the cost of estimating $u^{tRB}(\cdot, \cdot, \mu^{\text{test}})$ for n^{t-1} different μ^{test} , to the cost of running the FE code n^{t-1} times, and in this case even if the cost of the offline stage may be expensive, it will be amortized with the large dataset of size n^{t-1} that need to be constructed. In this work, we focus on the two-step reduction approach to approximate the time domain equation. Hence, we only emphasized above the operation count for the online stage of first step reduction and the second step reduction.

2.4. A posteriori Error Estimate for the Two-Step PR-RBC Method

Model order reduction techniques are generally certified with a posteriori error estimates, whose computation should not be expensive. Thus, these error estimates quantify the different between the solution obtained by the model order reduction technique and the high-fidelity one.

Proposition 1. Assume we do not have non-homogeneous Dirichlet boundary conditions and let $u^h(\cdot, \cdot, \mu)$ be the FE approximation to $u^l(\cdot, \cdot, \mu)$ solution to:

$$\left(\frac{\partial^n u^l(\cdot, t, \mu)}{\partial t^n}, v\right)_{L^2(\Omega)} + \sum_{i=0}^{n-1} a_i^l\left(\frac{\partial^i u^l(\cdot, t, \mu)}{\partial t^i}, v; \mu\right) = f^l(v, t; \mu), \quad \forall v \in X, \quad \forall t \in [0, T_{\text{sim}}], \quad (37)$$

where $n \geq 2$. Assume that $f^l(\cdot, \cdot; \mu)$ is a linear bounded form, that $a_i^l(\cdot, \cdot; \mu)$, $1 \leq i \leq n-1$, are bilinear forms and that the corresponding frequency domain bilinear forms $a_i(\cdot, \cdot; (\mu, \omega))$ are coercive such that $\forall \mu \in \mathcal{P}$, there exists $\alpha_i(\mu) > 0$ such that:

$$a_i(w, v; (\mu, \omega)) \geq \alpha_i(\mu, \omega)(w, v)_{L^2(\Omega)}, \quad \forall w, v \in X. \quad (38)$$

Then, if $u^{tRB}(\cdot, t, \mu)$ denotes the two-step PR-RBC approximation to $u^l(\cdot, \cdot, \mu)$ obtained using PR-RBC-Two-Step-Reduction algorithm (Algorithm 2) and if we assume that $\|f(\cdot, (\mu, \omega))\|_{V'}$ is bounded for $\omega \in [\omega_{\max}, +\infty[$, we have:

$$\begin{aligned} \|u^{th}(\cdot, t, \mu) - u^{tRB}(\cdot, t, \mu)\|_{L^2(\Omega)} &\leq \frac{\max_{\omega \in [\omega_{\max}, +\infty[} \|f(\cdot, (\mu, \omega))\|_{V'}}{\pi \times (n-1) \times \omega_{\max}^{n-1}} + \frac{1}{\pi} \left(\omega_{\max} \epsilon_{\text{SG}} + \int_0^{\omega_{\max}} \|u^h(\cdot, (\mu, \omega)) - u^{h, \mathbf{M}', \mathbf{N}}(\cdot, (\mu, \omega))\|_{L^2(\Omega)} d\omega \right) \\ &\leq \frac{\max_{\omega \in [\omega_{\max}, +\infty[} \|f(\cdot, (\mu, \omega))\|_{V'}}{\pi \times (n-1) \times \omega_{\max}^{n-1}} + \frac{\omega_{\max}}{\pi} \left(\epsilon_{\text{SG}} + \max_{\omega \in [0, \omega_{\max}] \|u^h(\cdot, (\mu, \omega)) - u^{h, \mathbf{M}', \mathbf{N}}(\cdot, (\mu, \omega))\|_{L^2(\Omega)} \right), \quad \forall t \in [0, T_{\text{sim}}] \end{aligned} \quad (39)$$

where ω_{\max} is an upper bound for the set Ξ_ω , $f(\cdot, \cdot)$ is the linear form of the frequency domain variational formulation 6, V' is the dual space of $L^2(\Omega)$ and ϵ_{SG} denotes the non normalized threshold corresponding to ϵ given as input to the SG-2nd-step-reduction algorithm (Algorithm 1).

PROOF OF PROPOSITION 1. Our error contains three terms: one related to the fact that when considering Ξ_ω we are actually taking into account only a truncated inverse Laplace transform, and two other terms, such that each of them is related to a specific reduction step among the two steps that we carry out. To quantify these terms, we introduce the FE based truncated inverse Laplace transform which has the following expression:

$$u_{[0, \omega_{\max}]}^{th}(\cdot, t, \mu) = \frac{1}{2\pi} \Re \left(\int_{-i\omega_{\max}}^{i\omega_{\max}} u^h(\cdot, (\mu, \omega)) e^{i\omega t} d\omega \right), \quad \forall t \in [0, T_{\text{sim}}]. \quad (40)$$

Then, we have:

$$\begin{aligned} \|u^{th}(\cdot, t, \mu) - u^{tRB}(\cdot, t, \mu)\|_{L^2(\Omega)} &= \|u^{th}(\cdot, t, \mu) - u_{[0, \omega_{\max}]}^{th}(\cdot, t, \mu) + u_{[0, \omega_{\max}]}^{th}(\cdot, t, \mu) - u^{tRB}(\cdot, t, \mu)\|_{L^2(\Omega)} \leq \\ &\|u^{th}(\cdot, t, \mu) - u_{[0, \omega_{\max}]}^{th}(\cdot, t, \mu)\|_{L^2(\Omega)} + \|u_{[0, \omega_{\max}]}^{th}(\cdot, t, \mu) - u^{tRB}(\cdot, t, \mu)\|_{L^2(\Omega)}, \forall t \in [0, T_{\text{sim}}], \end{aligned} \quad (41)$$

and

$$\begin{aligned} \|u^{th}(\cdot, t, \mu) - u_{[0, \omega_{\max}]}^{th}(\cdot, t, \mu)\|_{L^2(\Omega)} &= \\ \frac{1}{2\pi} \left\| \Re \left(\lim_{\omega' \rightarrow -\infty} \int_{-i\omega'}^{-i\omega_{\max}} u^h(\cdot, \mu_+) e^{i\omega t} d\omega + \lim_{\omega' \rightarrow \infty} \int_{i\omega_{\max}}^{i\omega'} u^h(\cdot, \mu_+) e^{i\omega t} d\omega \right) \right\|_{L^2(\Omega)}, \forall t \in [0, T_{\text{sim}}]. \end{aligned} \quad (42)$$

Since we have a real time domain variational form, we know that $u^h(\cdot, (\mu, -\omega)) = \overline{u^h(\cdot, (\mu, \omega))}$, where $\bar{\cdot}$ refers to the complex conjugate operator. The previous equality gives:

$$\|u^{th}(\cdot, t, \mu) - u_{[0, \omega_{\max}]}^{th}(\cdot, t, \mu)\|_{L^2(\Omega)} \leq \frac{1}{\pi} \lim_{\omega' \rightarrow \infty} \int_{i\omega_{\max}}^{i\omega'} \|u^h(\cdot, \mu_+)\|_{L^2(\Omega)} d\omega, \forall t \in [0, T_{\text{sim}}]. \quad (43)$$

To estimate the upper bound of the obtained inequality, we invoke the frequency domain variational form and plug in $u^h(\cdot, (\mu, \omega))$ as a test function to obtain:

$$(i\omega)^n \|u^h(\cdot, (\mu, \omega))\|_{L^2(\Omega)}^2 + \sum_{k=0}^{n-1} (i\omega)^k a_k(u^h, u^h, (\mu, \omega)) = f(u^h, (\mu, \omega)). \quad (44)$$

Using the coercivity of $a_k(\cdot, \cdot; (\mu, \omega))$, $1 \leq k \leq n-1$, we have:

$$\omega^n \|u^h(\cdot, (\mu, \omega))\|_{L^2(\Omega)}^2 \leq |(i\omega)^n \|u^h(\cdot, (\mu, \omega))\|_{L^2(\Omega)}^2 + \sum_{k=1}^{n-1} (i\omega)^k a_k(u^h, u^h, (\mu, \omega))|, \quad (45)$$

and thanks to the bounded linear form $f(u^h, (\mu, \omega))$, we have:

$$|f(u^h, (\mu, \omega))| \leq \|u^h(\cdot, (\mu, \omega))\|_{L^2(\Omega)} \times \|f(\cdot, (\mu, \omega))\|_{V'}. \quad (46)$$

The last three results give:

$$\|u^h(\cdot, (\mu, \omega))\|_{L^2(\Omega)} \leq \frac{\|f(\cdot, (\mu, \omega))\|_{V'}}{\omega^n}. \quad (47)$$

Since we assume that $\|f(\cdot, (\mu, \omega))\|_{V'}$ is bounded for $\omega \in [\omega_{\max}, +\infty[$, and that $n \geq 2$, using the previous inequality and (43), we obtain:

$$\|u^{th}(\cdot, t, \mu) - u_{[0, \omega_{\max}]}^{th}(\cdot, t, \mu)\|_{L^2(\Omega)} \leq \frac{\max_{\omega \in [\omega_{\max}, +\infty[} \|f(\cdot, (\mu, \omega))\|_{V'}}{\pi \times (n-1) \times \omega_{\max}^{n-1}}, \forall t \in [0, T_{\text{sim}}]. \quad (48)$$

Based on the inequality (41), the final step consists in estimating an upper bound for $\|u_{[0, \omega_{\max}]}^{th}(\cdot, t, \mu) - u^{tRB}(\cdot, t, \mu)\|_{L^2(\Omega)}$. We first write the difference using the truncated inverse Laplace transform:

$$u_{[0, \omega_{\max}]}^{th}(\cdot, t, \mu) - u^{tRB}(\cdot, t, \mu) = \frac{1}{2\pi} \Re \left(\int_{-i\omega_{\max}}^{i\omega_{\max}} (u^h(\cdot, (\mu, \omega)) - u^{tRB}(\cdot, (\mu, \omega))) e^{i\omega t} d\omega \right), \quad (49)$$

where $u^{tRB}(\cdot, (\mu, \omega))$ denotes the approximation of $u^h(\cdot, (\mu, \omega))$ obtained using X^{tRB} that we built in the second step reduction using SG-2nd-step-reduction algorithm (Algorithm 1). Then we have:

$$\begin{aligned} \|u^h(\cdot, (\mu, \omega)) - u^{tRB}(\cdot, (\mu, \omega))\|_{L^2(\Omega)} &= \|u^h(\cdot, (\mu, \omega)) - u^{h, \mathbf{M}', \mathbf{N}}(\cdot, (\mu, \omega)) + u^{h, \mathbf{M}', \mathbf{N}}(\cdot, (\mu, \omega)) - u^{tRB}(\cdot, (\mu, \omega))\|_{L^2(\Omega)} \leq \\ &\|u^h(\cdot, (\mu, \omega)) - u^{h, \mathbf{M}', \mathbf{N}}(\cdot, (\mu, \omega))\|_{L^2(\Omega)} + \|u^{h, \mathbf{M}', \mathbf{N}}(\cdot, (\mu, \omega)) - u^{tRB}(\cdot, (\mu, \omega))\|_{L^2(\Omega)} \leq \\ &\|u^h(\cdot, (\mu, \omega)) - u^{h, \mathbf{M}', \mathbf{N}}(\cdot, (\mu, \omega))\|_{L^2(\Omega)} + \epsilon_{\text{SG}}. \end{aligned} \quad (50)$$

Using the last two results, and again the property $u(\cdot, (\mu, -\omega)) = \overline{u(\cdot, (\mu, \omega))}$ since we have a real time domain variational form, we obtain:

$$\begin{aligned} \|u_{[0, \omega_{\max}]}^{ih}(\cdot, t, \mu) - u^{tRB}(\cdot, t, \mu)\|_{L^2(\Omega)} &\leq \frac{1}{\pi} \left(\omega_{\max} \epsilon_{SG} + \int_0^{\omega_{\max}} \|u^h(\cdot, (\mu, \omega)) - u^{h, M', N}(\cdot, (\mu, \omega))\|_{L^2(\Omega)} d\omega \right) \\ &\quad \frac{\omega_{\max}}{\pi} \left(\epsilon_{SG} + \max_{\omega \in [0, \omega_{\max}]} \|u^h(\cdot, (\mu, \omega)) - u^{h, M', N}(\cdot, (\mu, \omega))\|_{L^2(\Omega)} \right), \forall t \in [0, T_{\text{sim}}]. \end{aligned} \quad (51)$$

Combining (41), (48) and (51), we directly obtain the desired result (39). \square

Remarks:

1. $\|u^h(\cdot, (\mu, \omega)) - u^{h, M', N}(\cdot, (\mu, \omega))\|_{L^2(\Omega)}$ can be evaluated efficiently using a posteriori error estimates developed in previous works such as in [30].
2. $\|f(\cdot, (\mu, \omega))\|_{V'}$ can be computed efficiently since we assume that $f(\cdot, (\mu, \omega))$ is affine in the parameter (μ, ω) and thus the required parameter independent evaluations can be estimated within the offline stage of first step reduction. Moreover, a good choice of ω_{\max} generally guarantees that the spectrum of the load is continuously decreasing over $[\omega_{\max}, \infty[$, thus we generally have $\max_{\omega \in [\omega_{\max}, +\infty[} \|f(\cdot, (\mu, \omega))\|_{V'} = \|f(\cdot, (\mu, \omega_{\max}))\|_{V'}$ which is inexpensive to estimate.
3. Here we assumed that we do not have non-homogeneous Dirichlet boundary condition. This hypothesis can be removed and we would apply the previous result to the homogeneous part of the final solution, and we should add the error introduced by the POD approach to estimate the lift function corresponding to the non-homogeneous Dirichlet boundary condition which can be carried out efficiently since we simply apply a POD approximation to estimate such lift function.

Therefore, the a posteriori error estimate developed here is computationally inexpensive to estimate and thus can be computed along with the two-step PR-RBC-based approximation to the time domain solution.

2.5. Numerical Experiments

2.5.1. Wave Equation Non-homogeneous Neumann Boundary Condition

In this section, we apply the two-step PR-RBC approach detailed in the previous sections to the following scalar wave equation with damping for a domain Ω :

$$\nabla^2 u - \frac{L_{\text{ref}}^2}{c^2 \times T_{\text{ref}}^2} \frac{\partial^2 u}{\partial t^2} + \frac{\nu}{c_0^2 \times T_{\text{ref}}} \nabla^2 \frac{\partial u}{\partial t} = 0 \text{ in } \Omega, \quad (52)$$

$$u(x, t, \mu) = 0, \forall x \in \Sigma^D, \forall t > 0; \nabla u \cdot n = \mathcal{F}(x, t, \mu), \forall x \in \Sigma^N, \forall t > 0, \quad (53)$$

and

$$u(t = 0, x, \mu) = 0; \frac{\partial u}{\partial t}(t = 0, x, \mu) = 0, \forall x \in \Omega, \quad (54)$$

written in a dimensionless form. $c_0 > 0$ denotes the speed of sound in the medium considered, $c \in \mathbb{R}^*$ the wave speed and ν a damping coefficient that has the units of $\frac{L^2}{T}$ as a kinematic viscosity. n denotes the outer normal of Ω and let $\partial\Omega$ be partitioned such that $\partial\Omega = \Sigma^D \cup \Sigma^N$. T_{ref} is defined as: $T_{\text{ref}} \equiv \frac{L_{\text{ref}}}{c_0}$.

We consider the archetype components defined in figure 3. All the archetype components have the same rectangular geometry of length L and height H . We consider $L_{\text{ref}} = L$ and from now on, L and H will refer to the dimensionless lengths (which means that $L = 1$ but we will not omit L from the equations for sake of clarity).

We define the following archetype parameters and boundary conditions:

$$\hat{\mu}_1 \equiv (\nu, c, F_1, x_{c1}, \sigma_{x1}, \sigma_{t1}, \theta_1, F_2, x_{c2}, \sigma_{x2}, \sigma_{t2}, \theta_2), \quad (55)$$

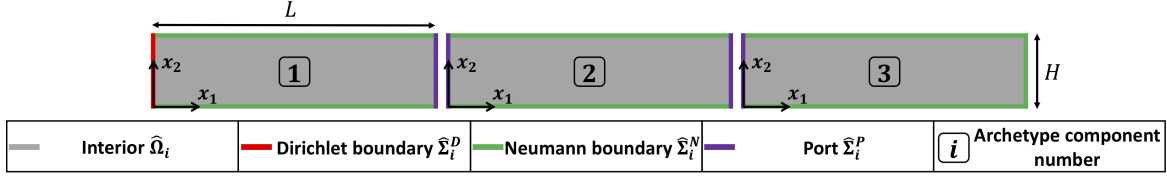


Figure 3: Archetype components anatomy for wave equation

$$\nabla u \cdot n = \hat{\mu}_{1;7} \times t \times e^{\frac{t}{\hat{\mu}_{1;6}}} \times \hat{\mu}_{1;3} \times e^{-\frac{(x_1 - \hat{\mu}_{1;4})^2}{\hat{\mu}_{1;5}^2}} \times \mathbb{1}_{\{x_2=H\}} + \hat{\mu}_{1;12} \times t \times e^{\frac{t}{\hat{\mu}_{1;11}}} \times \hat{\mu}_{1;8} \times e^{-\frac{(x_1 - \hat{\mu}_{1;9})^2}{\hat{\mu}_{1;10}^2}} \times \mathbb{1}_{\{x_2=H\}}, \quad \forall x \in \hat{\Sigma}_1^N; \quad (56)$$

$$\hat{\mu}_2 \equiv (\nu, c, F_1, x_{c1}, \sigma_{x1}, \sigma_{t1}, \theta_1, F_2, x_{c2}, \sigma_{x2}, \sigma_{t2}, \theta_2, F_3, x_{c3}, \sigma_{x3}, \sigma_{t3}, \theta_3), \quad (57)$$

$$\begin{aligned} \nabla u \cdot n = \hat{\mu}_{2;7} \times t \times e^{\frac{t}{\hat{\mu}_{2;6}}} \times \hat{\mu}_{2;3} \times e^{-\frac{(x_1 - \hat{\mu}_{2;4})^2}{\hat{\mu}_{2;5}^2}} \times \mathbb{1}_{\{x_2=H\}} + \hat{\mu}_{2;12} \times t \times e^{\frac{t}{\hat{\mu}_{2;11}}} \times \hat{\mu}_{2;8} \times e^{-\frac{(x_1 - \hat{\mu}_{2;9})^2}{\hat{\mu}_{2;10}^2}} \times \mathbb{1}_{\{x_2=H\}} + \\ \hat{\mu}_{2;17} \times t \times e^{\frac{t}{\hat{\mu}_{2;16}}} \times \hat{\mu}_{2;13} \times e^{-\frac{(x_1 - \hat{\mu}_{2;14})^2}{\hat{\mu}_{2;15}^2}} \times \mathbb{1}_{\{x_2=H\}}, \quad \forall x \in \hat{\Sigma}_2^N \end{aligned} \quad (58)$$

and

$$\hat{\mu}_3 \equiv (\nu, c, F_1, x_{c1}, \sigma_{x1}, \sigma_{t1}, \theta_1, F_2, x_{c2}, \sigma_{x2}, \sigma_{t2}, \theta_2), \quad (59)$$

$$\nabla u \cdot n = \hat{\mu}_{3;7} \times t \times e^{\frac{t}{\hat{\mu}_{3;6}}} \times \hat{\mu}_{3;3} \times e^{-\frac{(x_1 - \hat{\mu}_{3;4})^2}{\hat{\mu}_{3;5}^2}} \times \mathbb{1}_{\{x_2=H\}} + \hat{\mu}_{3;12} \times t \times e^{\frac{t}{\hat{\mu}_{3;11}}} \times \hat{\mu}_{3;8} \times e^{-\frac{(x_1 - \hat{\mu}_{3;9})^2}{\hat{\mu}_{3;10}^2}} \times \mathbb{1}_{\{x_2=H\}}, \quad \forall x \in \hat{\Sigma}_3^N. \quad (60)$$

By considering the Laplace transform and the augmented parameters $\hat{\mu}_{+j} \equiv (\hat{\mu}_j, \omega)$, where ω refers to the angular frequency, we obtain the following linear and bilinear forms for the frequency domain equation:

$$\hat{Q}_1^{a+} = 2; \quad \hat{\Theta}_{1;1}^{a+} = -\frac{L_{\text{ref}}^2 \times \hat{\mu}_{+1;13}^2}{\hat{\mu}_{+1;2}^2 \times T_{\text{ref}}^2}; \quad \hat{\Theta}_{1;2}^{a+} = +1 \frac{i \times \hat{\mu}_{+1;13} \times \hat{\mu}_{+1;1}}{c_0^2 \times T_{\text{ref}}^2}, \quad (61)$$

$$\hat{Q}_2^{a+} = 2; \quad \hat{\Theta}_{2;1}^{a+} = -\frac{L_{\text{ref}}^2 \times \hat{\mu}_{+2;18}^2}{\hat{\mu}_{+2;2}^2 \times T_{\text{ref}}^2}; \quad \hat{\Theta}_{2;2}^{a+} = 1 + \frac{i \times \hat{\mu}_{+2;18} \times \hat{\mu}_{+2;1}}{c_0^2 \times T_{\text{ref}}^2}, \quad (62)$$

$$\hat{Q}_3^{a+} = 2; \quad \hat{\Theta}_{3;1}^{a+} = -\frac{L_{\text{ref}}^2 \times \hat{\mu}_{+3;13}^2}{\hat{\mu}_{+3;2}^2 \times T_{\text{ref}}^2}; \quad \hat{\Theta}_{3;2}^{a+} = 1 + \frac{i \times \hat{\mu}_{+3;13} \times \hat{\mu}_{+3;1}}{c_0^2 \times T_{\text{ref}}^2}, \quad (63)$$

$$\hat{a}_{q;1}(u, v) = \int_{\hat{\Omega}_q} u \cdot \bar{v} \, dx; \quad \hat{a}_{q;2}(u, v) = \int_{\hat{\Omega}_q} \nabla u \cdot \bar{\nabla v} \, dx; \quad q \in \{1, 2, 3\}, \quad (64)$$

$$\hat{a}_q(\cdot, \cdot; \hat{\mu}_{+q}) = \sum_{r=1}^{\hat{Q}_q^{a+}} \hat{\Theta}_{q;r}^{a+}(\hat{\mu}_{+q}) \hat{a}_{q;r}(\cdot, \cdot); \quad q \in \{1, 2, 3\}, \quad (65)$$

$$\hat{f}_1(v; \hat{\mu}_{+1}) = \hat{\mu}_{+1;7} \times \hat{\mu}_{+1;3} \times \int_{\partial \hat{\Omega}_1} e^{-\frac{(x_1 - \hat{\mu}_{+1;4})^2}{\hat{\mu}_{+1;5}^2}} \times \mathbb{1}_{\{x_2=H\}} \times \bar{v} \, dx + \hat{\mu}_{+1;12} \times \hat{\mu}_{+1;8} \times \int_{\partial \hat{\Omega}_1} e^{-\frac{(x_1 - \hat{\mu}_{+1;9})^2}{\hat{\mu}_{+1;10}^2}} \times \mathbb{1}_{\{x_2=H\}} \times \bar{v} \, dx, \quad (66)$$

$$\begin{aligned} \hat{f}_2(v; \hat{\mu}_{+2}) = \hat{\mu}_{+2;7} \times \hat{\mu}_{+2;3} \times \int_{\partial \hat{\Omega}_2} e^{-\frac{(x_1 - \hat{\mu}_{+2;4})^2}{\hat{\mu}_{+2;5}^2}} \times \mathbb{1}_{\{x_2=H\}} \times \bar{v} \, dx + \hat{\mu}_{+2;12} \times \hat{\mu}_{+2;8} \times \int_{\partial \hat{\Omega}_2} e^{-\frac{(x_1 - \hat{\mu}_{+2;9})^2}{\hat{\mu}_{+2;10}^2}} \times \mathbb{1}_{\{x_2=H\}} \times \bar{v} \, dx + \\ \hat{\mu}_{+2;17} \times \hat{\mu}_{+2;13} \times \int_{\partial \hat{\Omega}_2} e^{-\frac{(x_1 - \hat{\mu}_{+2;14})^2}{\hat{\mu}_{+2;15}^2}} \times \mathbb{1}_{\{x_2=H\}} \times \bar{v} \, dx, \end{aligned} \quad (67)$$

and

$$\hat{f}_3(v; \hat{\mu}_{+3}) = \hat{\mu}_{+3;7} \times \hat{\mu}_{+3;3} \times \int_{\partial\hat{\Omega}_3} e^{-\frac{(x_1 - \hat{\mu}_{+3;4})^2}{\hat{\mu}_{+3;5}^2}} \times \mathbb{1}_{\{x_2=H\}} \times \bar{v} dx + \hat{\mu}_{+3;12} \times \hat{\mu}_{+3;8} \times \int_{\partial\hat{\Omega}_3} e^{-\frac{(x_1 - \hat{\mu}_{+3;9})^2}{\hat{\mu}_{+3;10}^2}} \times \mathbb{1}_{\{x_2=H\}} \times \bar{v} dx, \quad (68)$$

where $\bar{\cdot}$ refers to the complex conjugate operator. Hence, the variational formulation for the frequency domain equation for the archetype component $i \in \{1, 2, 3\}$ is given by the bilinear form $\hat{a}_i(\cdot, \cdot; \hat{\mu}_{+i})$ and the linear form $\hat{f}_i(\cdot; \hat{\mu}_{+i})$. For the linear forms $\hat{f}_q(\cdot; \hat{\mu}_{+q})$, $q \in \{1, 2, 3\}$, we use the EIM to recover the affine parametric dependence.

Using the archetype components, we consider the reference ports given in figure 4. The reference ports parameters and the boundary conditions considered for the associated pairwise component problem follow naturally from the parameters and the boundary conditions defined for the archetype components.

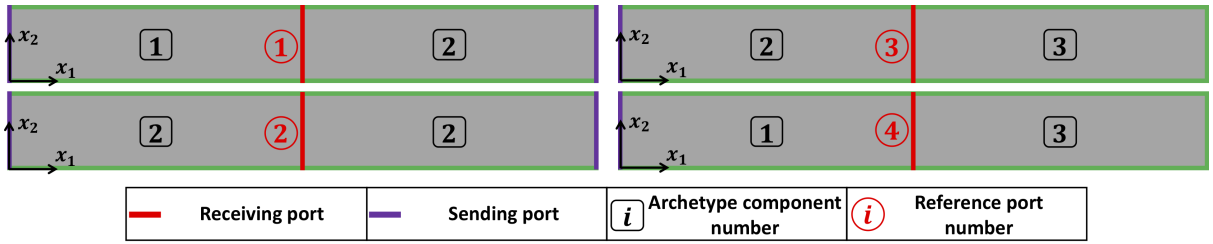


Figure 4: Reference ports (pairwise component) for wave equation

We take $L = 1.6$, $H = 1$ and consider the following parameters' probability density functions introduced for purpose of training:

$$\hat{\mu}_{+q;1} \sim \mathcal{U}([0.8 \times \bar{v}, 1.2 \times \bar{v}]); \bar{v} = 1.5111 \times 10^{-5} m^2.s^{-1}; q \in \{1, 2, 3\}, \quad (69)$$

$$\hat{\mu}_{+q;2} \sim \mathcal{U}([0.8 \times c_0, 1.2 \times c_0]); c_0 = 343 m.s^{-1}; q \in \{1, 2, 3\}, \quad (70)$$

$$\hat{\mu}_{+1;k} \sim \mathcal{U}([0.8, 1.2]); k \in \{3, 8\}, \quad (71)$$

$$\hat{\mu}_{+1;4} \sim \mathcal{U}([0, \frac{4}{5} \times L]), \quad (72)$$

$$\hat{\mu}_{+1;9} \sim \mathcal{U}([\frac{4}{5} \times L, \frac{6}{5} \times L]), \quad (73)$$

$$\hat{\mu}_{+1;k} \sim \mathcal{U}([0.8 \times \frac{L}{10}, 1.2 \times \frac{L}{10}]); k \in \{5, 10\}, \quad (74)$$

$$\hat{\mu}_{+1;k} \sim \mathcal{U}([0.8 \times \bar{\sigma}_t, 1.2 \times \bar{\sigma}_t]); \bar{\sigma}_t = 3; k \in \{6, 11\}, \quad (75)$$

$$\hat{\mu}_{+1;k} \sim \mathcal{U}([0, 1]); k \in \{7, 12\}, \quad (76)$$

$$\hat{\mu}_{+2;k} \sim \mathcal{U}([0.8, 1.2]); k \in \{3, 8, 13\}, \quad (77)$$

$$\hat{\mu}_{+2;4} \sim \mathcal{U}([\frac{-1}{5} \times L, \frac{1}{5} \times L]), \quad (78)$$

$$\hat{\mu}_{+2;9} \sim \mathcal{U}([\frac{1}{5} \times L, \frac{4}{5} \times L]), \quad (79)$$

$$\hat{\mu}_{+2;14} \sim \mathcal{U}([\frac{4}{5} \times L, \frac{6}{5} \times L]), \quad (80)$$

$$\hat{\mu}_{+2;k} \sim \mathcal{U}([0.8 \times \frac{L}{10}, 1.2 \times \frac{L}{10}]) ; k \in \{5, 10, 15\} , \quad (81)$$

$$\hat{\mu}_{+2;k} \sim \mathcal{U}([0.8 \times \bar{\sigma}_t, 1.2 \times \bar{\sigma}_t]) ; \bar{\sigma}_t = 3 ; k \in \{6, 11, 16\} , \quad (82)$$

$$\hat{\mu}_{+2;k} \sim \mathcal{U}(\{0, 1\}) ; k \in \{7, 12, 17\} , \quad (83)$$

$$\hat{\mu}_{+3;k} \sim \mathcal{U}([0.8, 1.2]) ; k \in \{3, 8\} , \quad (84)$$

$$\hat{\mu}_{+3;4} \sim \mathcal{U}([\frac{-1}{5} \times L, \frac{1}{5} \times L]) , \quad (85)$$

$$\hat{\mu}_{+3;9} \sim \mathcal{U}([\frac{1}{5} \times L, L]) , \quad (86)$$

$$\hat{\mu}_{+3;k} \sim \mathcal{U}([0.8 \times \frac{L}{10}, 1.2 \times \frac{L}{10}]) ; k \in \{5, 10\} , \quad (87)$$

$$\hat{\mu}_{+3;k} \sim \mathcal{U}([0.8 \times \bar{\sigma}_t, 1.2 \times \bar{\sigma}_t]) ; \bar{\sigma}_t = 3 ; k \in \{6, 11\} \quad (88)$$

and

$$\hat{\mu}_{+3;k} \sim \mathcal{U}(\{0, 1\}) ; k \in \{7, 12\} , \quad (89)$$

where $\mathcal{U}(\mathcal{T})$ refers to the uniform probability over interval \mathcal{T} . $c_0 = 343m.s^{-1}$ and $\bar{\nu} = 1.5111 \times 10^{-5}m^2.s^{-1}$ correspond to the celerity of sound in air and the kinematic viscosity of air at a temperature of $25^\circ C$ respectively. Note that if $\hat{\mu}_{+1;k} = 0$ for $k = 7$ and $k = 12$, then we randomly choose one of these two parameters to be equal to 1 for the archetype component 1's training. The same operation is considered for $\hat{\mu}_{+2;k} = 0$ for $k = 7$, $k = 12$ and $k = 17$ and for $\hat{\mu}_{+3;k} = 0$ for $k = 7$ and $k = 12$ for the other archetype components' training, so that we avoid null solutions. For the probability density functions used for pairwise component training, we consider the same ones as defined for the archetype components and we ensure that there is at least one nonzero load to avoid null solutions. We consider the following angular frequency discretization based on $\bar{\sigma}_t$:

$$\hat{\mu}_{+1;13}, \hat{\mu}_{+2;18}, \hat{\mu}_{+3;13} \in \{0, d\omega, \dots, \omega_{\max}\} , d\omega = \frac{0.2}{\bar{\sigma}_t} , \omega_{\max} = \frac{10}{\bar{\sigma}_t} . \quad (90)$$

The sizes of the different reduced bases formed at the first step reduction are chosen based on the decrease of the eigenvalues of the transfer eigenvalue problem and the decrease of the POD modes for the reduced bubble space for inhomogeneity, the reduced port space and for the reduced space for port-mode lifting. Table 1 gather the sizes of the different reduced bases and the computation time to run the offline stage of first step reduction. All simulations considered in this work were run on a 4-core laptop (with a 3.5 GHz Intel CPU and 16 GB RAM).

Size of training set	51
Size of port spaces	$\hat{M}_1 = \hat{M}_2 = 6$ $\hat{M}_3 = \hat{M}_4 = 5$
Size of bubble spaces for port-mode lifting	$\hat{N}_{k,m,\ell} = 4, 1 \leq k \leq 4, 1 \leq m \leq \hat{M}_k, \ell = 1, 2$
Size of of bubble space for inhomogeneity	$\hat{N}_1^{\text{inhom}} = \hat{N}_3^{\text{inhom}} = 11$ $\hat{N}_2^{\text{inhom}} = 12$
Computation time to run offline stage of 1 st step reduction	11.75s

Table 1: PR-RBC reduced bases sizes for wave equation with inhomogeneous Neumann BC

We consider the global model consisting of $n_{\text{comp}} = 5$ components and given in figure 5. The time domain variational problem for such model has a total of 55 parameters, while the frequency domain variational problems have either 11 or 15 parameters for the archetype components, and 17, 21 or 25 parameters regarding the reference ports. These local parameters associated with the frequency domain variational problems define the parameters' spaces considered in building the reduced bases within the two-step PR-RBC method. Those sizes are considerably

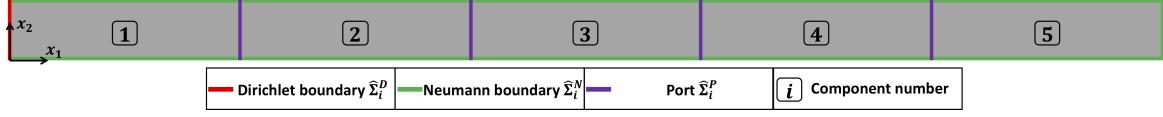


Figure 5: Global model for wave equation with inhomogeneous Neumann BC

lower than the parameter space's size of the global domain and thus it shows how the two-step PR-RBC method solves the issue of curse of dimensionality by reducing the effective dimensionality of the parameter spaces considered in the variational problems to approximate. The parameter spaces' dimension reduction becomes more significant when the global model contains more components as it will be the case for the second numerical experiment detailed in section 2.5.2.

We then run the PR-RBC-Two-Step-Reduction algorithm (Algorithm 2) with $T_{\text{sim}} = 10$ and $N_t = 10^4$. The size of the reduced space $\underline{\mathcal{X}}^{\text{RB}}$ is fixed such that the time domain relative error between the two-step approach-based solution and the FE approximation is below 1% for 10 randomly sampled parameters and two parameters for which the values are taken equal to the extremes of the interval considered in the probability density functions. The relative error for the time domain solutions that we consider here is defined as:

$$\frac{\|u^{t\text{RB}}(\cdot, t, \mu^{\text{test}}) - u^{th}(\cdot, t, \mu^{\text{test}})\|_{H^1(\Omega)}}{\frac{1}{T_{\text{sim}}} \int_0^{T_{\text{sim}}} \|u^{th}(\cdot, t, \mu^{\text{test}})\|_{H^1(\Omega)} dt}.$$

Table 2 gathers the average computation time to run the major steps of the PR-RBC-Two-Step-Reduction algorithm (Algorithm 2) for the parameters considered to compute the relative error. The size of $\underline{\mathcal{X}}^{\text{RB}}$ needed to satisfy our criteria regarding the time domain relative error between the two-step PR-RBC and the FE approximation is equal to 12. The size of the full \mathbb{P}_2 FE approximation space is equal to $N^h = 3739$ and computing one full FE simulation takes 190s on average.

PR-RBC-1st-step-reduction-Online algorithm called $n_\omega = 51$ times	0.25 s
SG-2nd-step-reduction (Algorithm 1)	0.05 s
Time marching	0.22 s
Total computation time to run PR-RBC-Two-Step-Reduction algorithm (Algorithm 2)	0.52 s

Table 2: Computation time of the PR-RBC-Two-Step-Reduction algorithm for wave equation with inhomogeneous Neumann BC

Hence, the two-step reduction approach has a computation cost 365 times lower than the FE simulation for this example. Figure 6 gives the evolution of the relative error in time:

$$\frac{\|u^{t\text{RB}}(\cdot, t, \mu^{\text{test}}) - u^{th}(\cdot, t, \mu^{\text{test}})\|_{H^1(\Omega)}}{\frac{1}{T_{\text{sim}}} \int_0^{T_{\text{sim}}} \|u^{th}(\cdot, t, \mu^{\text{test}})\|_{H^1(\Omega)} dt},$$

for the parameter such that we apply only one load with amplitude equal to $F = 1$, centered at $x_c = \frac{n_{\text{comp}} \times L}{2}$, with a spatial width $\sigma_x = \frac{L}{10}$ and with the temporal parameter $\sigma_t = \frac{9}{\pi}$. We note $L_{\text{tot}} = n_{\text{comp}} \times L$. The kinematic viscosity and wave speed are taken equal to $\bar{\nu}$ and c_0 respectively for all components. We see well that this error does not exceed 1% over the simulation time.

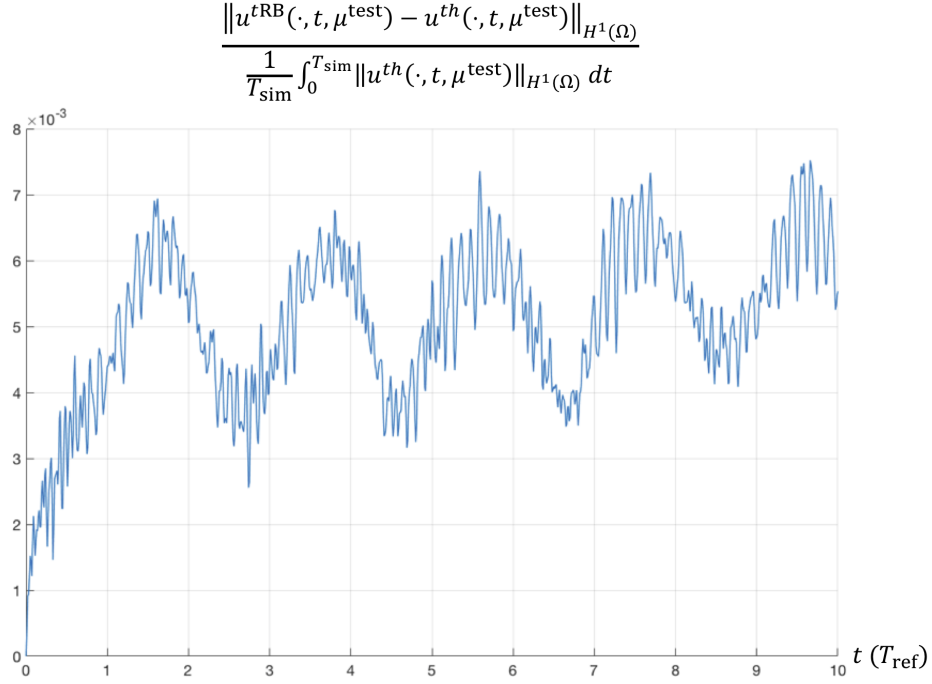


Figure 6: Time domain relative error for equation with inhomogeneous Neumann BC

2.5.2. Elastodynamic Equation Example

In this section, we apply the two-step PR-RBC approach to the following 2D elastodynamic PDE for an isotropic material with damping over a domain Ω :

$$\frac{\partial^2 u}{\partial t^2} + C^{\text{damp}} \left(\frac{\partial u}{\partial t} \right) + \frac{E \times T_{\text{ref}}^2}{\rho \times L_{\text{ref}}^2} \mathcal{L}(u) = 0 \text{ in } \Omega, \quad (91)$$

$$\mathcal{L}(u) = -\text{div}(\sigma(u)); \sigma(u) = \frac{1}{1+\nu} \text{sym}(\nabla u) + \frac{\nu}{(1+\nu)(1-2\nu)} \text{div}(u) \mathbb{I}, \quad (92)$$

$$C^{\text{damp}}(\nu) \equiv \alpha_{\text{Ray}} \times T_{\text{ref}} \times \nu + \frac{\beta_{\text{Ray}} \times E \times T_{\text{ref}}^2}{\rho \times L_{\text{ref}}^2} \mathcal{L}(\nu), \quad (93)$$

$$u(x, t, \mu) = 0, \forall x \in \Sigma^D, \forall t > 0; \sigma(u) \cdot n = \mathcal{F}_\mu(x, t, \mu), \forall x \in \Sigma^N, \forall t > 0, \quad (94)$$

$$u(t = 0, x, \mu) = 0; \frac{\partial u}{\partial t}(t = 0, x, \mu) = 0, \forall x \in \Omega, \quad (95)$$

written in a dimensionless form, where $u \in \mathbb{R}^2$ is the displacement field. ν denotes the Poisson ratio, $\rho > 0$ the material density, $\alpha_{\text{Ray}} > 0$ and $\beta_{\text{Ray}} > 0$ the Rayleigh damping coefficients and $E > 0$ the Young's modulus. n denotes the outer normal of Ω and $\partial\Omega$ is assumed to be partitioned such that $\partial\Omega = \Sigma^D \cup \Sigma^N$. T_{ref} is defined as: $T_{\text{ref}} \equiv \frac{L_{\text{ref}}}{c_t}$, where $c_t = \sqrt{\frac{\bar{E}}{2 \times \rho \times (1+\bar{\nu})}}$ is the celerity of the transverse wave in infinite domain without damping. \bar{E} and $\bar{\nu}$ refer to fixed values taken as reference for the Young modulus and the Poisson ratio respectively, and which have an order of magnitude similar to the values that are taken by E and ν respectively.

We consider a bridge with a moving 2-axle vehicle. In our model, we consider the vehicle-bridge interaction to be the most significant at the connection between the bridge's decks, since this region generally presents gaps and

metallic connectors and thus the vehicle's passing in such region induces vibrations that propagate through the bridge. Therefore, we neglect the vehicle-bridge interaction at other regions than the bridge's decks connection.

To simulate the bridge model described above, we consider the archetype components defined in figure 7. The archetype components 1 and 5 have a rectangular geometry of dimension $\frac{3}{2}L \times H$ and contain a Dirichlet boundary each. The archetype components 3 and 4 have also a rectangular geometry of dimension $L \times H$ and do not contain any Dirichlet boundary. Component 3 has only homogeneous Neumann boundary conditions, while component 4 will model the connection between the decks and thus has a non-homogeneous Neumann boundary condition as detailed below. The archetype component number 2 has a T shape with thickness equal to H and whose dimensions are given in figure 7. Finally, the archetype component number 6 has a rectangular geometry of dimension $L \times H$ with non-homogeneous Neumann boundary condition but also contain a crack whose dimensions are detailed in figure 7. This archetype component can be used along with the archetype component 4 to model the existence or not of damage within a context of Simulation Based Classification for Structural Health Monitoring for instance. We consider $L_{\text{ref}} = H$ and from now on, L and H will refer to the dimensionless lengths (which means that $H = 1$ but we will not omit H from the equations for sake of clarity).

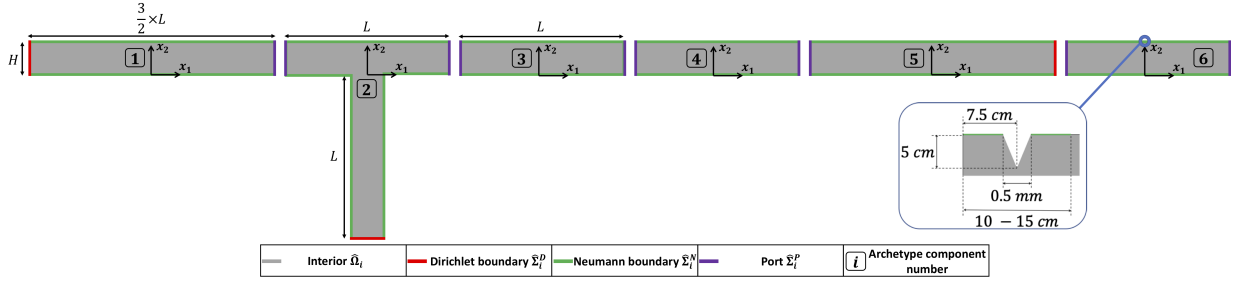


Figure 7: Archetype components anatomy for elastodynamic bridge considered for SBC

We define the following archetype parameters and boundary conditions:

$$\hat{\mu}_q \equiv (\alpha_{\text{Ray}}, \beta_{\text{Ray}}, E), q \in \{1, 2, 3, 5\}, \quad (96)$$

$$\hat{\mu}_q \equiv (\alpha_{\text{Ray}}, \beta_{\text{Ray}}, E, F, x_c, \sigma_x, f, d_1, d_2), q \in \{4, 6\}. \quad (97)$$

$$u(x, t, \hat{\mu}_q) = 0, \forall x \in \hat{\Sigma}_q^D, q \in \{1, 2\}, \quad (98)$$

$$\sigma(u) \cdot n = 0, \forall x \in \hat{\Sigma}_q^N, q \in \{1, 2, 3, 5\}, \quad (99)$$

and

$$\sigma(u) \cdot n = \begin{bmatrix} \hat{\mu}_{q;7} \times \hat{\mu}_{q;4} \times e^{-\frac{(x_1 - \hat{\mu}_{q;5})^2}{\hat{\mu}_{q;6}^2}} \times \mathbb{1}_{\{x_2=H\}} \times \mathbb{1}_{\{x_1 \geq -\hat{\mu}_{q;8}\}} \times \mathbb{1}_{\{x_1 \leq \hat{\mu}_{q;9}\}} \\ -\hat{\mu}_{q;4} \times e^{-\frac{(x_1 - \hat{\mu}_{q;5})^2}{\hat{\mu}_{q;6}^2}} \times \mathbb{1}_{\{x_2=H\}} \times \mathbb{1}_{\{x_1 \geq -\hat{\mu}_{q;8}\}} \times \mathbb{1}_{\{x_1 \leq \hat{\mu}_{q;9}\}} \end{bmatrix}, \forall x \in \hat{\Sigma}_q^N, q \in \{4, 6\}. \quad (100)$$

By considering the Laplace transform and the augmented parameters $\hat{\mu}_{+q} \equiv (\hat{\mu}_q, \omega)$, where ω refers to the angular frequency, we obtain the following linear and bilinear forms for the frequency domain equation:

$$\hat{Q}_q^{a+} = 2, q \in \{1, \dots, 6\}, \quad (101)$$

$$\hat{\Theta}_{q;1}^{a+} = -\hat{\mu}_{+q;4}^2 + iT_{\text{ref}} \times \hat{\mu}_{+q;1} \times \hat{\mu}_{+q;4}, q \in \{1, 2, 3, 5\}, \quad (102)$$

$$\hat{\Theta}_{q;2}^{a+} = \frac{T_{\text{ref}}}{\rho \times L_{\text{ref}}^2} \times \hat{\mu}_{+q;3} \times (T_{\text{ref}} + i \times \hat{\mu}_{+q;2} \times \hat{\mu}_{+q;4}), q \in \{1, 2, 3, 5\}, \quad (103)$$

$$\hat{\Theta}_{q;1}^{a+} = -\hat{\mu}_{+q;10}^2 + iT_{\text{ref}} \times \hat{\mu}_{+q;1} \times \hat{\mu}_{+q;10}, q \in \{4, 6\}, \quad (104)$$

$$\hat{\Theta}_{q,2}^{a+} = \frac{T_{\text{ref}}}{\rho \times L_{\text{ref}}^2} \times \hat{\mu}_{+q;3} \times (T_{\text{ref}} + i \times \hat{\mu}_{+q;2} \times \hat{\mu}_{+q;10}), q \in \{4, 6\}, \quad (105)$$

$$\hat{a}_{q,1}(u, v) = \int_{\hat{\Omega}_q} u \cdot \bar{v} \, dx, \quad q \in \{1, \dots, 6\}, \quad (106)$$

$$\begin{aligned} \hat{a}_{q,2}(u, v) &= \frac{\nu}{(1+\nu) \times (1-2\nu)} \times \int_{\hat{\Omega}_j} \frac{\partial u_i}{\partial x_j} \frac{\partial \bar{v}_k}{\partial x_l} \delta_{ik} \delta_{jl} \, dx + \frac{1}{2(1+\nu)} \times \int_{\hat{\Omega}_q} \frac{\partial u_i}{\partial x_j} \frac{\partial \bar{v}_k}{\partial x_l} (\delta_{ik} \delta_{jl} + \delta_{il} \delta_{jk}) \, dx = \\ &= \frac{\nu}{(1+\nu) \times (1-2\nu)} \times \int_{\hat{\Omega}_q} \text{div}(u) \cdot \overline{\text{div}(v)} \, dx + \frac{1}{1+\nu} \times \int_{\hat{\Omega}_q} \text{sym}(\nabla u) : \overline{\text{sym}(\nabla v)} \, dx, \quad q \in \{1, \dots, 6\}, \end{aligned} \quad (107)$$

$$\hat{f}_q(v; \hat{\mu}_{+q}) = 0, \quad q \in \{1, 2, 3, 5\}, \quad (108)$$

and

$$\begin{aligned} \hat{f}_q(v; \hat{\mu}_{+q}) &= -\hat{\mu}_{+q;4} \times \int_{\partial \hat{\Omega}_q} e^{-\frac{(x_1 - \hat{\mu}_{+q;5})^2}{\hat{\mu}_{+q;6}^2}} \times \mathbb{1}_{\{x_2=H\}} \times \mathbb{1}_{\{x_1 \geq -\hat{\mu}_{q;8}\}} \times \mathbb{1}_{\{x_1 \leq \hat{\mu}_{q;9}\}} \times \bar{v}_2 \, dx + \\ &= \hat{\mu}_{+q;7} \times \hat{\mu}_{+q;4} \times \int_{\partial \hat{\Omega}_q} e^{-\frac{(x_1 - \hat{\mu}_{+q;5})^2}{\hat{\mu}_{+q;6}^2}} \times \mathbb{1}_{\{x_2=H\}} \times \mathbb{1}_{\{x_1 \geq -\hat{\mu}_{q;8}\}} \times \mathbb{1}_{\{x_1 \leq \hat{\mu}_{q;9}\}} \times \bar{v}_1 \, dx +, \quad q \in \{4, 6\}, \end{aligned} \quad (109)$$

where $\bar{\cdot}$ refers to the complex conjugate and in the expressions of $\hat{a}_{q,2}(\cdot, \cdot)$, for $q \in \{1, \dots, 6\}$, we used the Einstein summation notation. Hence, the variational formulation for the frequency domain equation for the archetype component $i \in \{1, \dots, 6\}$ is given by the bilinear form $\hat{a}_i(\cdot, \cdot; \hat{\mu}_{+i})$ and the linear form $\hat{f}_i(\cdot; \hat{\mu}_{+i})$. Its well-posedness follows from Korn's inequality.

Using the archetype components, we consider the reference port given in figure 8. The reference port parameter and the boundary conditions considered for the associated pairwise component problem follow naturally from the parameters and the boundary conditions defined for the archetype components.

We take $L = 5$, $H = 1$ and consider the following parameters' probability density functions introduced based on literature review:

$$\hat{\mu}_{+q;1} \sim \mathcal{U}([a_{\text{Ray}}^{\min}, a_{\text{Ray}}^{\max}]), \quad q \in \{1, \dots, 6\}, \quad (110)$$

$$\hat{\mu}_{+q;2} \sim \mathcal{U}([\beta_{\text{Ray}}^{\min}, \beta_{\text{Ray}}^{\max}]), \quad q \in \{1, \dots, 6\}, \quad (111)$$

$$\hat{\mu}_{+q;3} \sim \mathcal{U}([E_{\min}, E_{\max}]), \quad q \in \{1, \dots, 6\}, \quad (112)$$

$$\hat{\mu}_{+q;4} \sim \mathcal{U}([F_{\min}, F_{\max}]), \quad q \in \{4, 6\}, \quad (113)$$

$$\hat{\mu}_{+q;5} \sim \mathcal{U}([-d_{\max} - 2 \times \sigma_x^{\max}, d_{\max} + 2 \times \sigma_x^{\max}]), \quad q \in \{4, 6\}, \quad (114)$$

$$\hat{\mu}_{+q;6} \sim \mathcal{U}([\sigma_x^{\min}, \sigma_x^{\max}]), \quad q \in \{4, 6\}, \quad (115)$$

$$\hat{\mu}_{+q;7} \sim \mathcal{U}([f_{\min}, f_{\max}]), \quad q \in \{4, 6\}, \quad (116)$$

$$\hat{\mu}_{+q;8}, \hat{\mu}_{+q;9} \sim \mathcal{U}([d_{\min}, d_{\max}]), \quad q \in \{4, 6\}, \quad (117)$$

where $\mathcal{U}(\mathcal{T})$ refers to the uniform probability over interval \mathcal{T} . We choose reinforced concrete as material since it is one of the most used materials in building bridges. Thus, we take $\alpha_{\text{Ray}}^{\min} = 0.566 \, s^{-1}$, $\alpha_{\text{Ray}}^{\max} = 4.311 \, s^{-1}$, $\beta_{\text{Ray}}^{\min} = 0.009 \, s$ and $\beta_{\text{Ray}}^{\max} = 0.021 \, s$ as established in [33] for highway bridges in concrete. We also have $E_{\min} = 29 \, GPa$ and $E_{\max} = 37 \, GPa$ as determined in [34] for reinforced concrete. We take $\bar{E} = \frac{E_{\min} + E_{\max}}{2}$. The spatial dependence of the tire-road contact pressure was chosen based on the results obtained in [35] and [36], which show profiles close to moving Gaussians with $\sigma_x^{\min} = 2 \, cm$, $\sigma_x^{\max} = 4 \, cm$, $F_{\min} = 10^6 \, Pa$ and $F_{\max} = 2 \times 10^6 \, Pa$. Based on [35] (and also using <https://www.engineeringtoolbox.com>), we can estimate the friction coefficient between a typical car tire and asphalt such that $f_{\min} = 0.5$ and $f_{\max} = 0.7$. The distance along which we apply the load, and thus the span of the region defining the connection between the bridge's decks (characterized by the parameters $\hat{\mu}_{+q;8}, \hat{\mu}_{+q;9}$ for $q \in \{4, 6\}$),

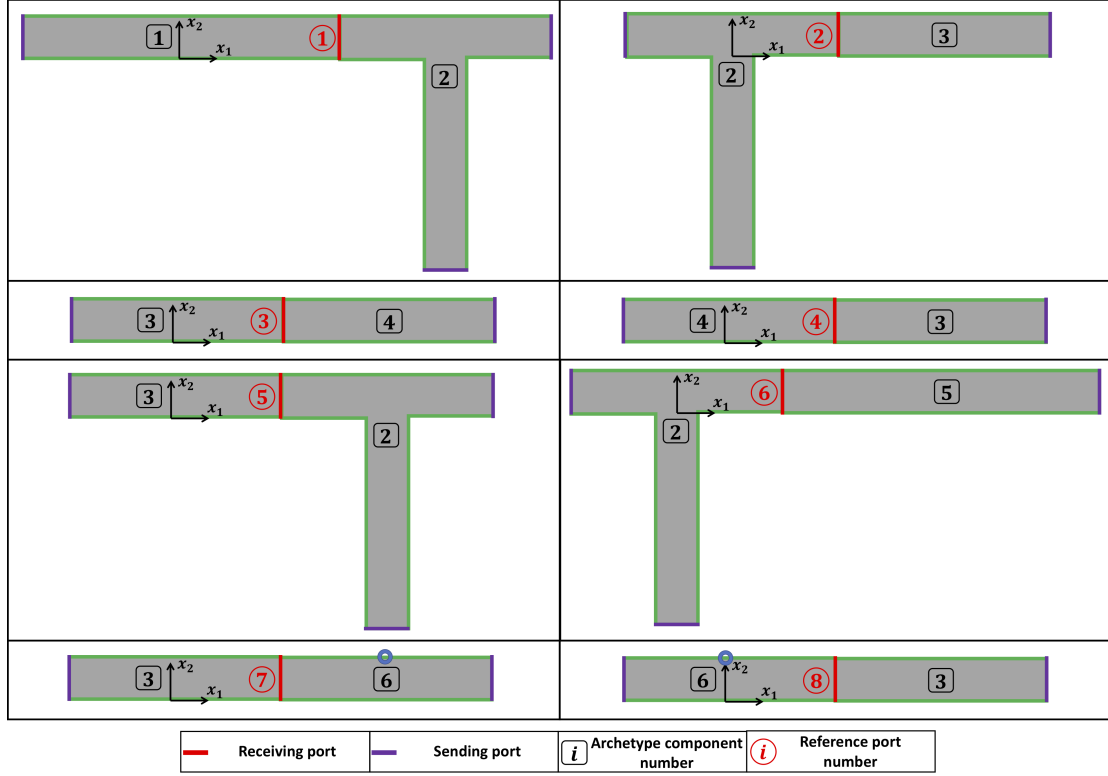


Figure 8: Reference port (pairwise component) for elastodynamic bridge considered for SBC

is determined by $d_{\min} = 10 \text{ cm}$ and $d_{\max} = 15 \text{ cm}$ based on [37] that gives the details of the possible connection options for prefabricated bridge elements in reinforced concrete. Moreover, the geometry of the crack for component 6 was fixed such that it has the maximum allowable dimensions fixed by Federal Highway Administration of the U.S. Department of Transportation [38], [39]. Finally, for reinforced concrete, we set $\rho = 2400 \text{ kg.m}^{-3}$ and $\nu = 0.15$ [40] (using <https://www.engineeringtoolbox.com> and <https://www.concrete.org/>).

For the probability density functions used for pairwise component training, we consider the same ones as defined for the archetype components. Since we are modeling a moving vehicle, to determine the characteristic time, and thus angular frequency, of our load, we need first to estimate the vehicle's speed. We consider vehicles with speed between $V_{\min} = 15 \text{ km.h}^{-1}$ and $V_{\max} = 50 \text{ km.h}^{-1}$, and thus we have the following angular frequency discretization, based on the vehicle's speed and the distance along which we apply the load:

$$\hat{\mu}_{+q;4}, \hat{\mu}_{+q';10} \in \{0, d\omega, \dots, \omega_{\max}\}, \quad q \in \{1, 2, 3, 5\}, \quad q' \in \{4, 6\}, \quad d\omega = \frac{V_{\min}}{2 \times d_{\max}}, \quad \omega_{\max} = 10 \times \frac{V_{\max}}{2 \times d_{\min}}. \quad (118)$$

The sizes of the different reduced bases formed at the first step reduction are chosen based on the decrease of the eigenvalues of the transfer eigenvalue problem and the decrease of the POD modes for the reduced bubble space for inhomogeneity, the reduced port space and for the reduced space for port-mode lifting. Table 3 gathers the sizes of the different reduced bases and the computation time to run the offline stage of first step reduction. All simulations considered in this work were run on a 4-core laptop (with a 3.5 GHz Intel CPU and 16 GB RAM).

For instance, figure 9 shows the convergence of the eigenvalues of the transfer eigenvalue problem for the reference port number 1 and a randomly sampled parameter $\hat{\mu}_{+1}^P$ from the training set, and the convergence of the POD eigenvalues for port-mode reduction to form the reduced port space, that we chose to be of size $\hat{M}_1 = 3$. Figure 10

Size of training set	51
Size of port spaces	$\hat{M}_k = 3, k = 1, 2, 5, 6$ $\hat{M}_k = 4, k = 3, 4, 7, 8$
Size of bubble spaces for port-mode lifting	$\hat{N}_{k,m,\ell} = 2, 1 \leq k \leq 8, 1 \leq m \leq \hat{M}_k$
Size of of bubble space for inhomogeneity	$\hat{N}_i^{\text{inhom}} = 1, i = 4, 6$
Computation time to run offline stage of 1 st step reduction	128s

Table 3: PR-RBC reduced bases sizes for elastodynamic cross considered for SBC

shows the decrease of the POD eigenvalues for the construction of reduced space for port-mode liftings for the 1st port-mode retained for the reference port number 8 within the two archetype components connected through it. We chose the corresponding reduced bubble spaces for port-mode liftings to be of size $\hat{N}_{8,1,\ell} = 2, \ell = 1, 2$. In figure 11, we give the convergence of the POD eigenvalues for construction of bubble space for inhomogeneity for archetype component number 4.

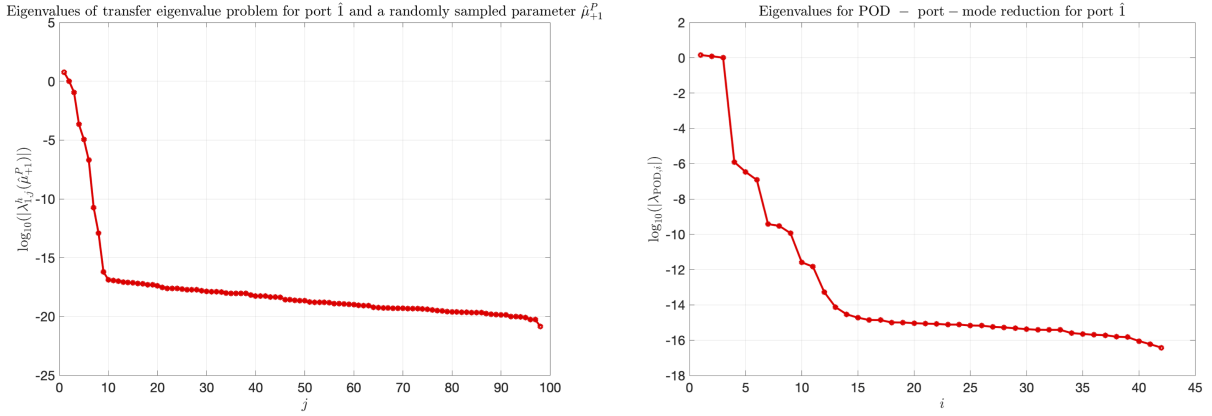


Figure 9: Convergence of the eigenvalues of the transfer eigenvalue problem for the reference port 1 and a randomly sampled parameter $\hat{\mu}_{+1}^P$, and convergence of the POD eigenvalues for port-mode reduction

We consider the global model consisting of 23 components and given in figure 12. The mapping of each component to the corresponding archetype one is given in table 4. Since each of components number 8 and 16 can have a crack, they are either mapped to the archetype component 4 or 6.

Component number in global model	Archetype component number
1	1
23	5
3, 5, 7, 9, 11, 13, 15, 17, 19, 21	3
2, 6, 10, 14, 18, 22	2
4, 12, 20	4
8, 16	4 or 6

Table 4: PR-RBC reduced bases sizes for elastodynamic bridge considered for SBC

For the time domain equation, we have to consider two more parameters for the global domain: the vehicle speed V and the distance between the two axles noted d_a . d_a follows a Gaussian probability density function with mean

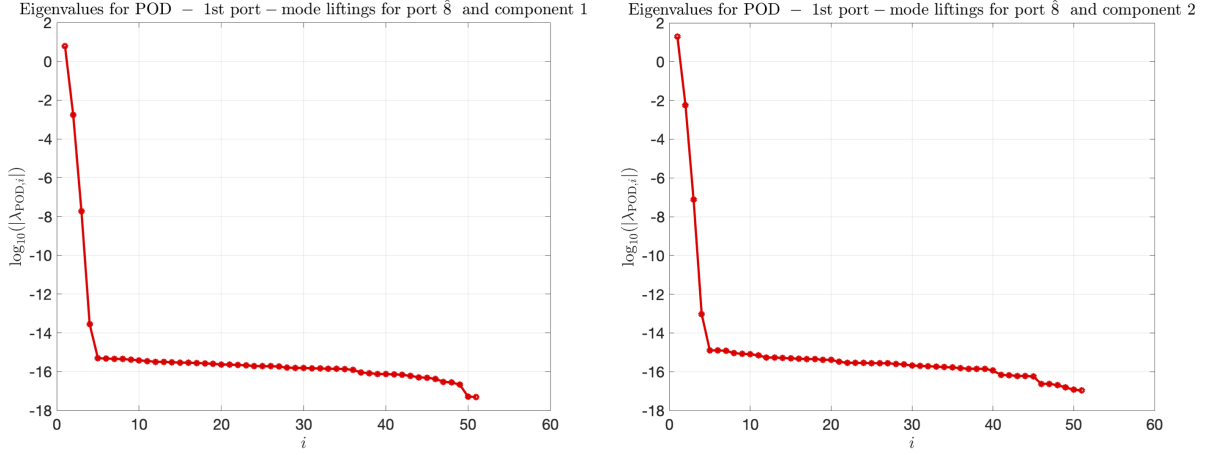


Figure 10: Convergence of the POD eigenvalues for constructing the reduced space for port-mode liftings for the 1st port-mode retained for the reference port number 8

equal to $\overline{d_a} = 3 \text{ m}$ and a standard deviation equal to $\sigma_{d_a} = 0.5 \text{ m}$ based on generic dimensions of 2-axle vehicles, while V is sampled from a uniform probability density function define over $[V_{\min}, V_{\max}]$. Figure 13 illustrates this with the moving gaussian profiles of the loads applied on the bridge once the vehicle's tires are within one of the decks' connections. The time domain variational problem for such model has a total of 89 parameters, while the frequency domain variational problems have either 4 or 10 parameters for the archetype components, and 7 or 13 parameters regarding the reference ports. These local parameters associated with the frequency domain variational problems define the parameters' spaces considered in building the reduced bases within the two-step PR-RBC method. Those sizes are considerably lower than the parameter space's size of the global domain and thus it shows how the two-step PR-RBC method solves the issue of curse of dimensionality by reducing the effective dimensionality of the parameter spaces considered in the variational problems to approximate.

We then run the PR-RBC-Two-Step-Reduction algorithm (Algorithm 2) with $N_t = 2 \times 10^3$. The simulation time T_{sim} is fixed based on the vehicle's speed V such that we allow it to travel across the bridge. The size of the reduced space $\underline{\underline{\mathcal{X}}}^{\text{RB}}$ is fixed based on the a posteriori error estimate (39) and by verifying that the time domain relative error between the two-step approach-based solution and the FE approximation is below 1% for 10 randomly sampled parameters and two parameters for which the values are taken equal to the extremes of the interval considered in the probability density functions. The relative error for the time domain solutions that we consider here is defined as:

$$\frac{\|u^{\text{tRB}}(\cdot, t, \mu^{\text{test}}) - u^{\text{th}}(\cdot, t, \mu^{\text{test}})\|_{H^1(\Omega)}}{\max_{t \in [0, T_{\text{sim}}]} \|u^{\text{th}}(\cdot, t, \mu^{\text{test}})\|_{H^1(\Omega)}}.$$

Table 5 gathers the average computation time to run the major steps of the PR-RBC-Two-Step-Reduction algorithm (Algorithm 2) for the parameters considered to compute the relative error. The size of $\underline{\underline{\mathcal{X}}}^{\text{RB}}$ needed to satisfy our criteria regarding the time domain relative error between the two-step PR-RBC and the FE approximation is equal to 30. The size of the full \mathbb{P}_2 FE approximation space is equal to $N^h = 17532 \pm 36$ and computing one full FE simulation takes 215s on average.

Hence, the two-step reduction approach has a computation cost 58 times lower than the FE simulation for this example. In the context of Simulation Based Classification for Structural Health Monitoring, construction of datasets of size of the order of 10^4 are often required to obtain satisfactory classification results. Conducting such task for this bridge example using the two-step PR-RBC approach has a total computation time of 10.67 hours (taking into account

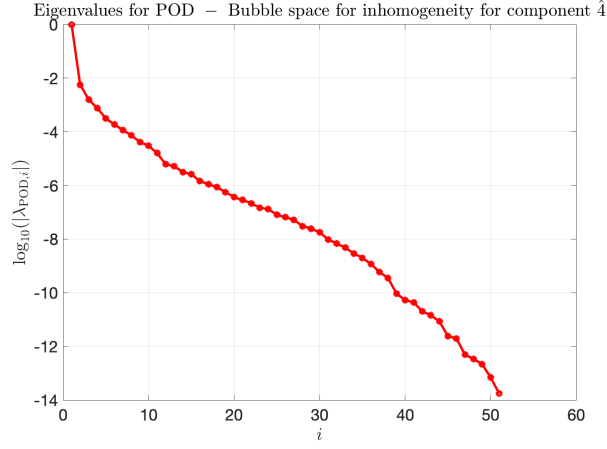


Figure 11: Convergence of the POD eigenvalues for constructing the bubble space for inhomogeneity for archetype component number 4

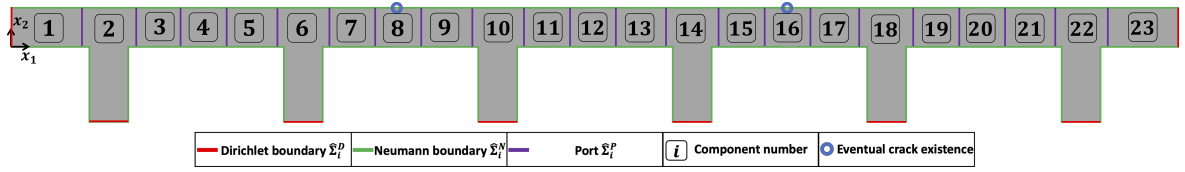


Figure 12: Global model for elastodynamic bridge (frequency domain PDE)

the computational cost of the offline stage of the 1st step reduction, which is run only once), instead of estimated 24.88 days using full FE space. Figure 14 gives the evolution of the exact error in time:

$$\|u^{tRB}(\cdot, t, \mu) - u^{th}(\cdot, t, \mu)\|_{L^2(\Omega)},$$

with the a posteriori error estimate:

$$\Delta(\mu) := \frac{\max_{\omega \in [\omega_{\max}, +\infty[} \|f(\cdot, (\mu, \omega))\|_{V'}}{\pi \times (n-1) \times \omega_{\max}^{n-1}} + \frac{\omega_{\max}}{\pi} \left(\epsilon_{SG} + \max_{\omega \in [0, \omega_{\max}]} \|u^h(\cdot, (\mu, \omega)) - u^{h, \mathbf{M}^*, \mathbf{N}}(\cdot, (\mu, \omega))\|_{L^2(\Omega)} \right),$$

in dashed line for the following four cases:

1. Case 1: all parameters are equal to their average value (average of their probability density functions) and we don't have any crack (components 8 and 16 are both mapped to archetype component 4).

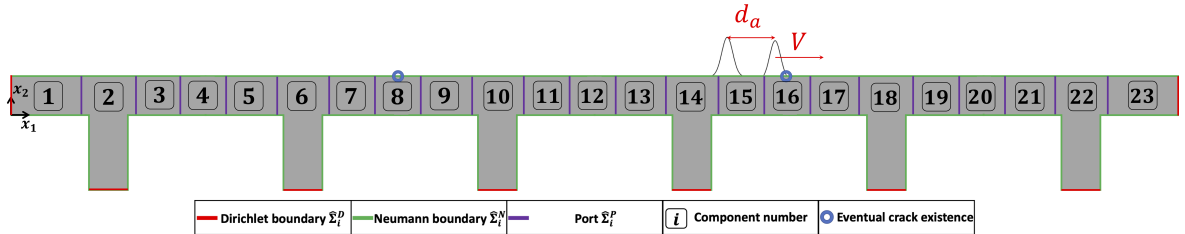


Figure 13: Global model for elastodynamic bridge (time domain PDE)

PR-RBC-1st-step-reduction-Online algorithm called $n_\omega = 51$ times	2.92s
SG-2nd-step-reduction (Algorithm 1)	0.56s
Time marching	0.25s
Total computation time to run PR-RBC-Two-Step-Reduction algorithm (Algorithm 2)	3.73s

Table 5: Computation time of the PR-RBC-Two-Step-Reduction algorithm for elastodynamic bridge considered for SBC

- Case 2: all parameters are equal to their average value and component 8 has a crack (component 8 is thus mapped to the archetype component 6, while component 16 is mapped to the archetype component 4).
- Case 3: all parameters, except d_a , are equal to their minimum allowable values which consist in the lower bound of the intervals used for the uniform probability density functions and $d_a = \bar{d}_a - 4 \times \sigma_{d_a}$. Component 16 has a crack (component 8 is thus mapped to the archetype component 4, while component 16 is mapped to the archetype component 6).
- Case 4: all parameters, except d_a , are equal to their maximum allowable values which consist in the upper bound of the intervals used for the uniform probability density functions and $d_a = \bar{d}_a + 4 \times \sigma_{d_a}$. We also consider 2 cracks (component 8 and 16 are both mapped to the archetype component 6).

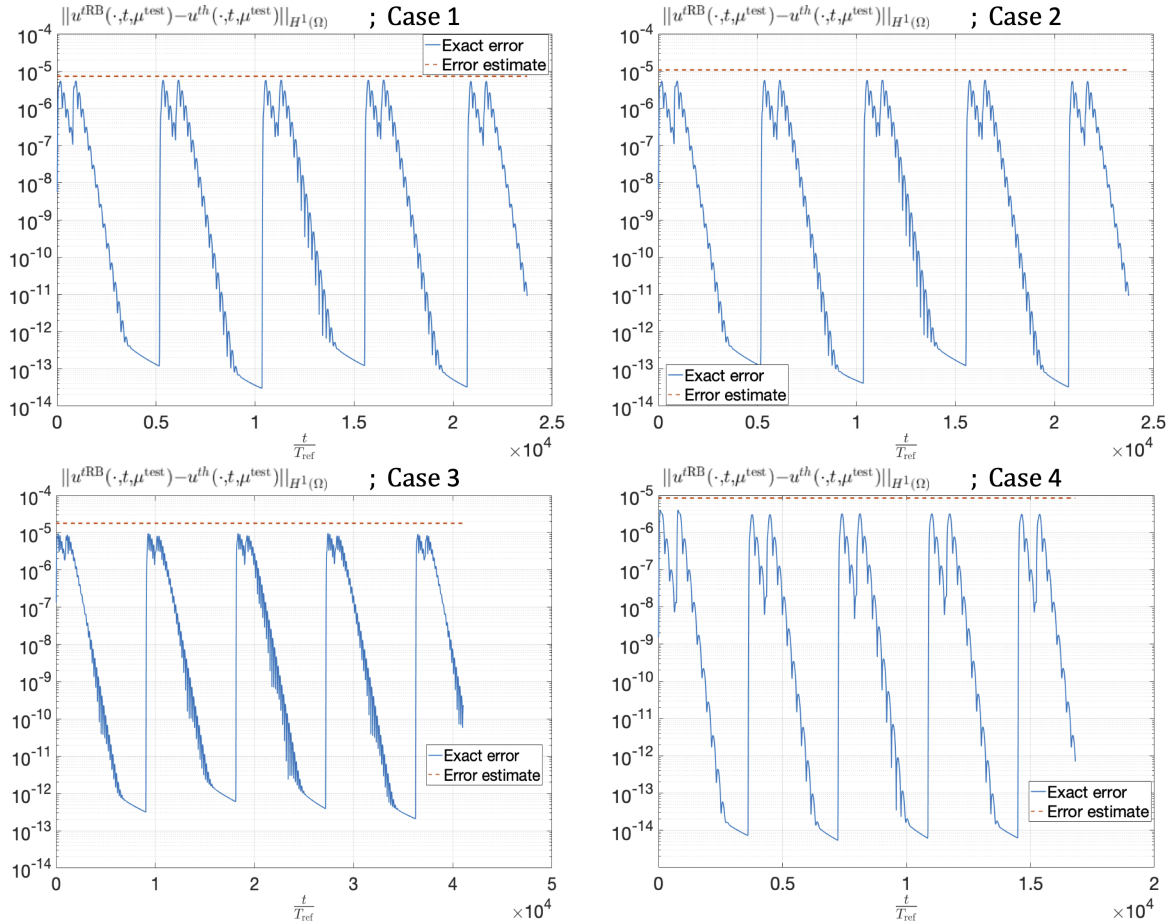


Figure 14: Exact time domain error and a posteriori error estimate for elastodynamic bridge

To quantify the performance of the a posteriori error estimate, we also compute the ratio:

$$\frac{\Delta(\mu)}{\max_{t \in [0, T_{\text{sim}}]} \|u^{\text{tRB}}(\cdot, t, \mu) - u^{\text{th}}(\cdot, t, \mu)\|_{L^2(\Omega)}},$$

whose value gets closer to 1 as the a posteriori error gives better estimate of the actual error. This ratio has the following values for the four cases detailed previously:

1. Case 1: $\frac{\Delta(\mu)}{\max_{t \in [0, T_{\text{sim}}]} \|u^{\text{tRB}}(\cdot, t, \mu) - u^{\text{th}}(\cdot, t, \mu)\|_{L^2(\Omega)}} = 1.17$,
2. Case 2: $\frac{\Delta(\mu)}{\max_{t \in [0, T_{\text{sim}}]} \|u^{\text{tRB}}(\cdot, t, \mu) - u^{\text{th}}(\cdot, t, \mu)\|_{L^2(\Omega)}} = 1.67$,
3. Case 3: $\frac{\Delta(\mu)}{\max_{t \in [0, T_{\text{sim}}]} \|u^{\text{tRB}}(\cdot, t, \mu) - u^{\text{th}}(\cdot, t, \mu)\|_{L^2(\Omega)}} = 2.01$,
4. Case 4: $\frac{\Delta(\mu)}{\max_{t \in [0, T_{\text{sim}}]} \|u^{\text{tRB}}(\cdot, t, \mu) - u^{\text{th}}(\cdot, t, \mu)\|_{L^2(\Omega)}} = 2.13$,

which shows the good performance of the a posteriori error estimate as $\Delta(\mu)$ and $\max_{t \in [0, T_{\text{sim}}]} \|u^{\text{tRB}}(\cdot, t, \mu) - u^{\text{th}}(\cdot, t, \mu)\|_{L^2(\Omega)}$ have the same order of magnitude and their ratio takes value typically bounded by 2.5 for the cases considered.

Figure 15 gives the evolution of the time domain relative error between the two-step approach-based solution and the FE approximation for the four cases detailed above, and we can verify that it is well below 1%. Figure 16 gives the convergence of the strong greedy algorithm (Algorithm 1) for the same four cases detailed above. We also provide in figures 17 and 18 the two-step PR-RBC-based solution and its difference with the full FE solution obtained at a fixed point for cases 1 and 2 defined above. The error is two orders of magnitude lower than the solution. Note that the obtained waves correspond well to the dispersive flexural waves but since for reinforced concrete the damping terms are not negligible compared to the mass and stiffness ones, we obtain damped flexural waves. We verify well that for 0 damping we recover the “well-known” (non-damped) dispersive flexural waves. Finally, figure 19 gives the two-step PR-RBC-based solution in space and its difference with the full FE solution obtained for case 4 detailed above, at a fixed time step chosen such that the vehicle is at the midpoint of the bridge’s length. As before, the error is two orders of magnitude lower than the actual solution.

3. Conclusion

3.1. Summary

This work presents the development of a parametrized Model Order Reduction (pMOR) approach to approximate hyperbolic time domain Partial Differential Equations (PDEs) for large domain with localized source terms and/or local parameters variation.

The two-step Port-Reduced Reduced-Basis Component method (PR-RBC) takes advantage of the time-frequency duality such that the PR-RBC reduced bases are built for the frequency domain PDE obtained by Laplace transform of the time domain equation. This guarantees the possibility of constructing relatively low-dimensional spaces able to well approximate the elliptic frequency domain PDE, instead of approximating the hyperbolic time domain problem. Moreover, considering the frequency domain PDE lets us get rid of the time dimension. Therefore, instead of approximating a manifold spanned by the possible trajectories followed by the time domain solutions, we approximate the manifold spanned by the solutions to static problems in which we have to account for the frequency as an additional parameter, which is considerably less challenging than the first option. This strategy also results in an offline stage of first step reduction that has significantly lower computational cost.

In addition, the two-step PR-RBC approach is a static condensation procedure based on domain decomposition and thus it solves the issue of curse of dimensionality by reducing the effective dimensionality of the parameter spaces considered in the variational problems to approximate. Therefore, the two-step PR-RBC approach addresses not a

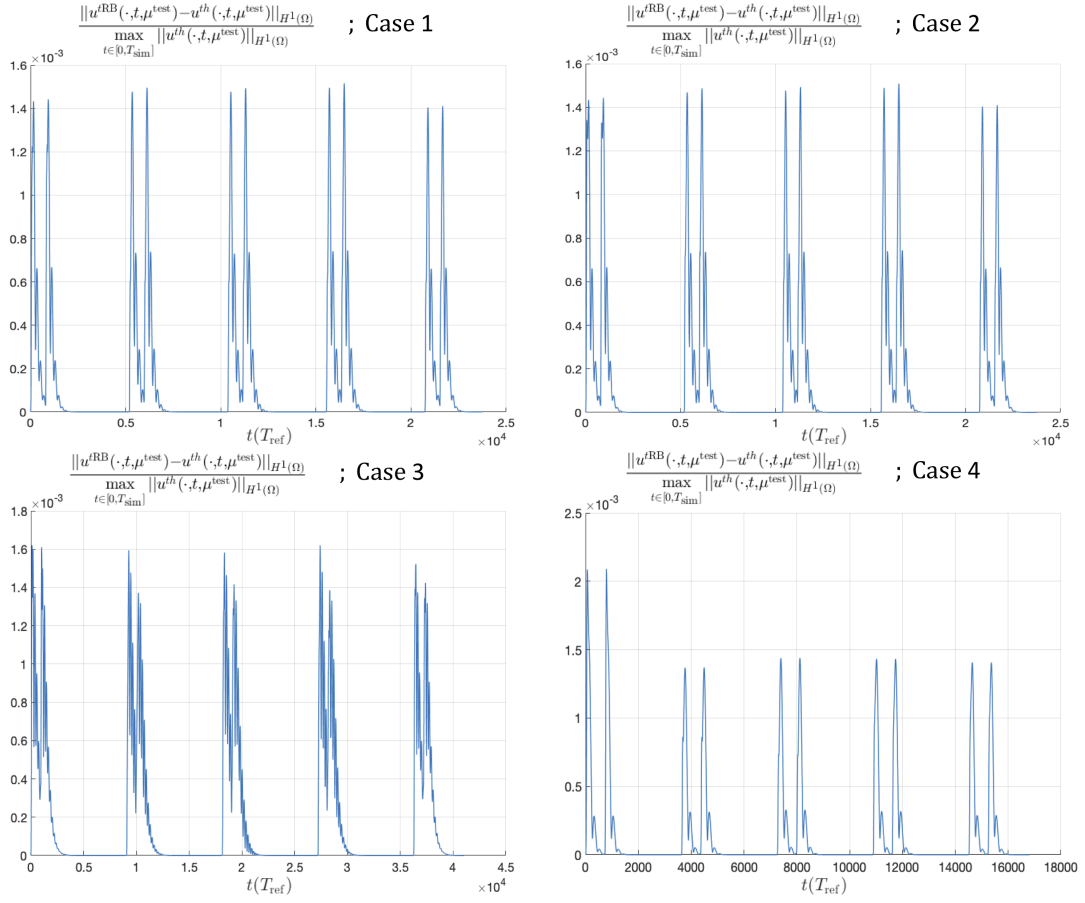


Figure 15: Time domain relative error for elastodynamic bridge considered for SBC - error normalized by the maximum norm of FE solution in time

particular global model but a family of global models through a common physical discipline and hence PDE operator and also typically some unifying engineering context. Moreover, we took advantage of the transfer eigenvalue problem to construct the port modes, since it is an optimal local approximation space for the behavior of the solution on the ports.

To approximate the time domain PDE for a global domain, we rely on a two-step strategy.

- First, we use the PR-RBC bases to compute the global frequency domain solutions at well selected frequencies: this corresponds to the first step reduction.
- Second, we consider these solutions as high-fidelity approximation and use them to form a final reduced basis to approximate the global time domain solution: this corresponds to the second step of reduction that we carry out through a strong greedy approach.

The efficiency of our method relies on the fact that the time domain solution is the inverse Laplace transform of a frequency domain function which is the solution to the frequency domain PDE. Thus, we can approximate the time domain solution as linear combination of the final reduced basis obtained for the frequency domain PDE. Therefore, for the time solver, we simply project our time domain equation on the final reduced space within which we carry out the time marching. We used the two-step PR-RBC approach to solve the wave equation and the elastodynamic equation applied to a bridge example, which can be considered for a simulation-based classification task for structural

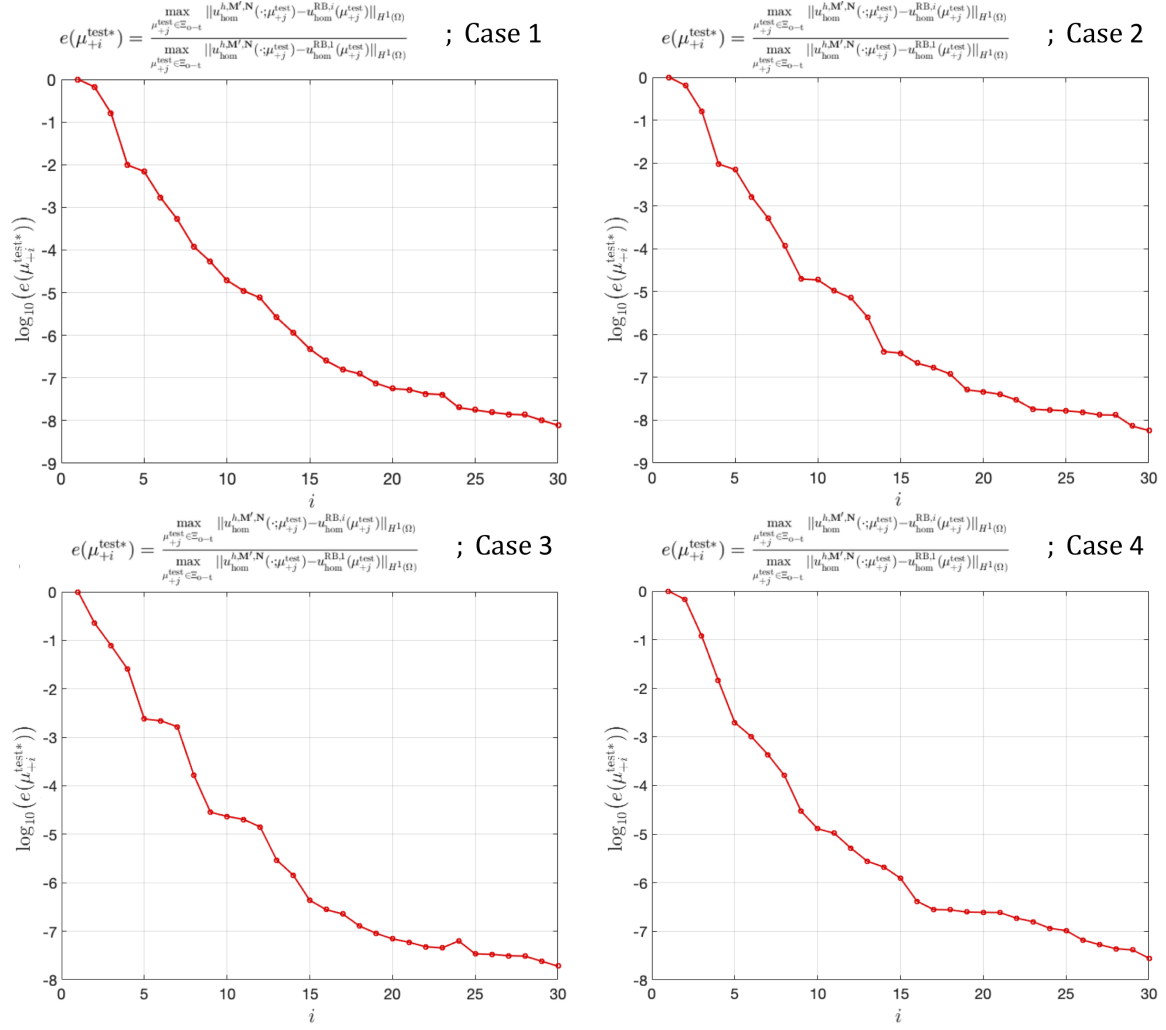


Figure 16: Strong Greedy algorithm (Algorithm 1) convergence for elastodynamic bridge considered for SBC

health monitoring. Finally, we also provide an a posteriori error estimate for the two-step PR-RBC approach based on the time-frequency duality. Such error estimate is computationally inexpensive, and hence it can be computed within the online stage to provide an error indicator along with the computation of the two-step PR-RBC-based approximation.

3.2. Future Work

In a future work, we will show the usefulness of the two-step PR-RBC method in the context of Simulation Based Classification (SBC) for Structural Health Monitoring (SHM) of deployed mechanical structures.

Moreover, our two-step PR-RBC method — based on the time-frequency duality via the Laplace transform and on the static condensation procedure that we followed — relied on the assumption that the underlined time domain PDE was linear. Some work has been done recently on domain decomposition reduced order modeling of non-linear PDE such as on using local hypersurfaces [41]. However, extending the port reduction method to non-linear PDEs would significantly increase the range of applications to which the technique can be applied and we could thus compare it

with the existing procedures for such problems. This extension should also include stability analysis and a posteriori error estimate development.

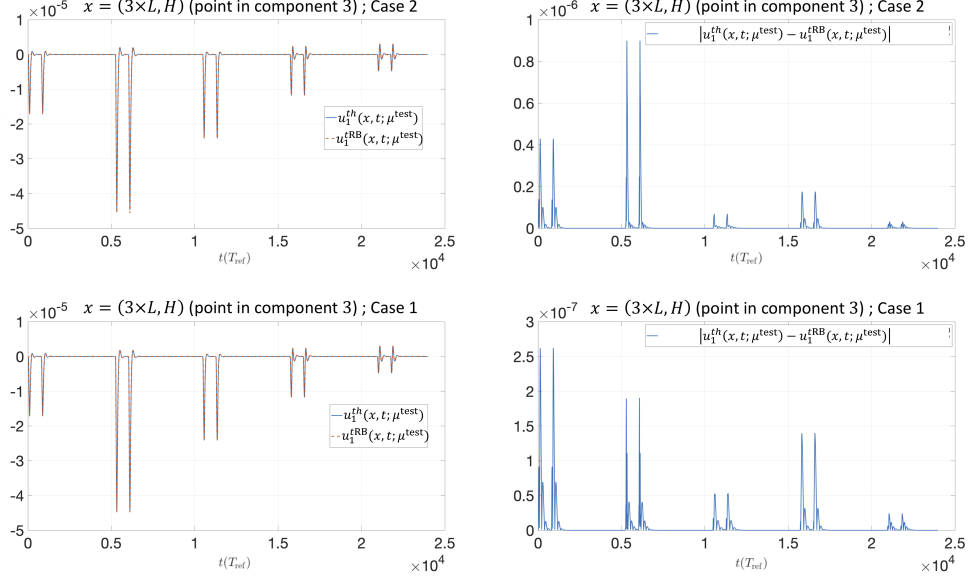


Figure 17: PR-RBC-based solution for displacement u_1 and difference with FE solution at point $(3 \times L, H)$ for cases 1 and 2

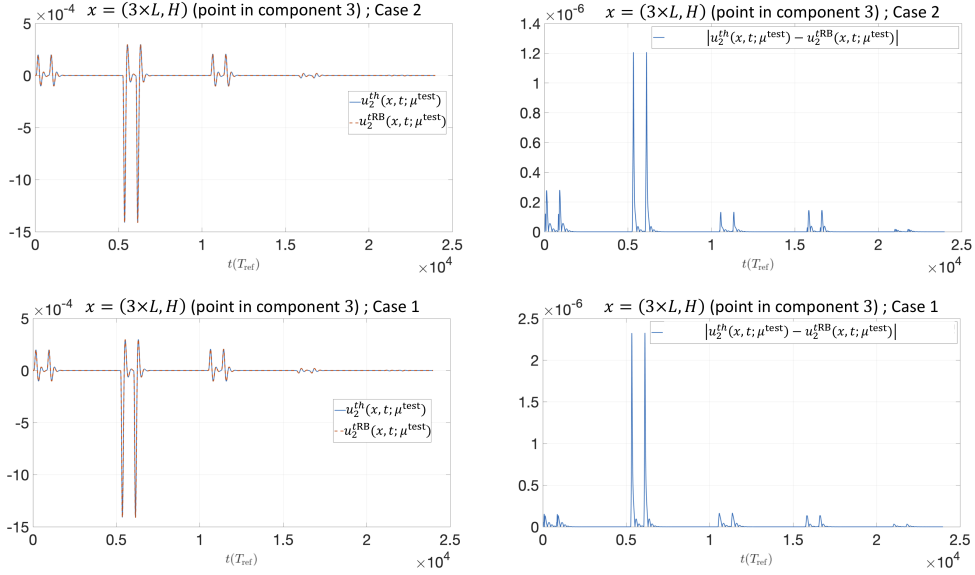


Figure 18: PR-RBC-based solution for displacement u_2 and difference with FE solution at point $(3 \times L, H)$ for cases 1 and 2

Plots for t such that the vehicle is at bridge's midpoint ; Case 4

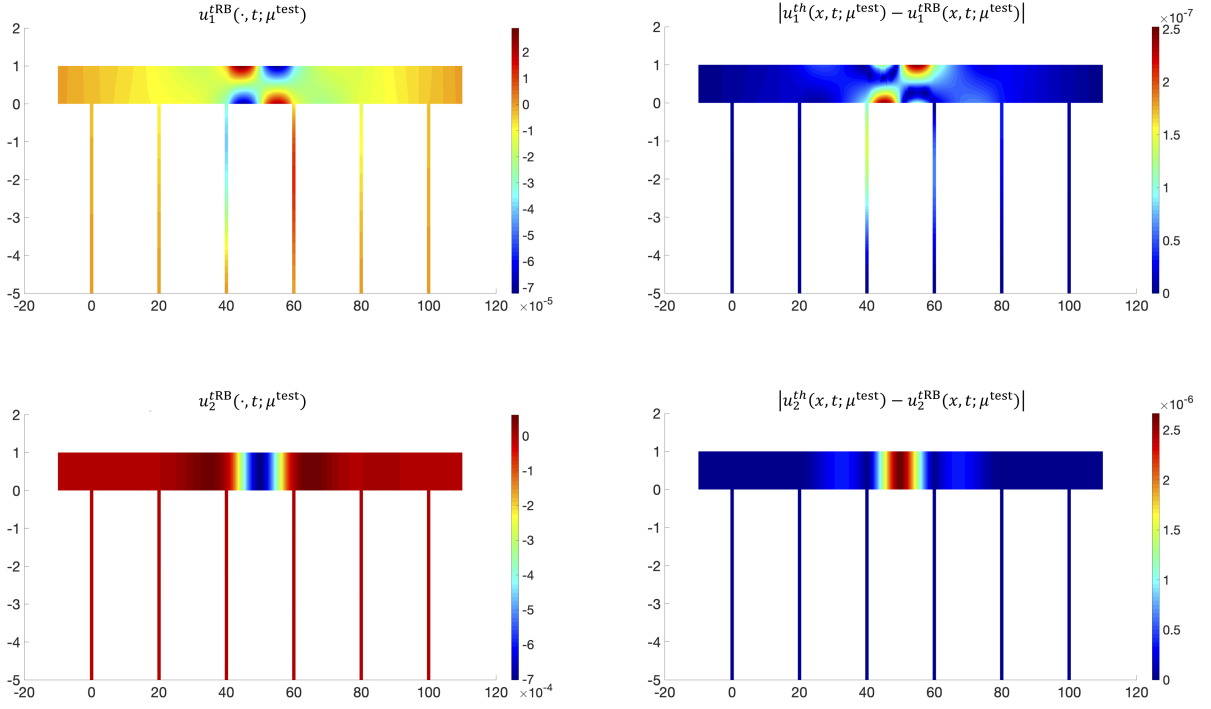


Figure 19: PR-RBC-based solution in space and difference with FE solution at fixed time for case 4

4. Acknowledgments

We would like to thank Professor Anthony T. Patera, Dr. Tommaso Taddei and Professor Masayuki Yano for the helpful software they provided us with. In terms of implementation, we resort to a 2D continuous-Galerkin Finite Element solver. Our implementation is based on a suite of Matlab codes [42] that has been developed by Professor Masayuki Yano (University of Toronto) during his stay at MIT.

Appendix A. Algorithms

Algorithm 1 SG-2nd-step-reduction algorithm

```

1: function SG-2ND-STEP-REDUCTION( $\mu^{\text{test}}, \Xi_\omega, n_\omega, \mathcal{N}^h, \underline{\underline{X}}^{h, \text{norm}}, \mathcal{I}, \epsilon, N, \{\varphi_j, 1 \leq j \leq \mathcal{N}^h\}, Q^{a+}, Q^{f+},$ 
    $\{\Theta_r^{a+}(\cdot), 1 \leq r \leq Q^{a+}\}, \{\Theta_r^{f+}(\cdot), 1 \leq r \leq Q^{f+}\}, \{\underline{\underline{\mathcal{A}}}^h, 1 \leq r \leq Q^{a+}\}, \{\underline{\underline{\mathcal{F}}}^h, 1 \leq r \leq Q^{f+}\})$ 
2:    $\Xi_{0-1} \leftarrow \{\mu_{+j}^{\text{test}} \equiv (\mu^{\text{test}}, \omega_j); \omega_j \in \Xi_\omega, 1 \leq j \leq n_\omega\}$ 
3:    $i \leftarrow 0$ 
4:    $\underline{\underline{X}}^{\text{RB}} \leftarrow []$ 
5:    $\underline{\underline{i}}_g \leftarrow \text{randi}(n_\omega)$ 
6:    $I_g \leftarrow []$ 
7:    $\underline{\underline{e}} \leftarrow 0_{N+1}$ 
8:    $\underline{\underline{e}}(1) \leftarrow \epsilon + 1$ 
9:    $\underline{\underline{r}}_0 \leftarrow 0_{n_\omega}$ 
10:   $\underline{\underline{r}} \leftarrow 0_{n_\omega}$ 
11:   $\underline{\underline{Z}} \leftarrow 0_{\mathcal{N}^{hND} \times n_\omega}$ 
12:   $\underline{\underline{\mathcal{D}}}^{\text{RB}} \leftarrow []$ 
13:   $\underline{\underline{\mathcal{D}}}^{\text{RB}} \leftarrow []$ 
14:  for  $r := 1$  to  $Q^{a+}$  do
15:     $\underline{\underline{\mathcal{A}}}^{\text{RB}} \leftarrow []$ 
16:  end for
17:  for  $r := 1$  to  $Q^{f+}$  do
18:     $\underline{\underline{\mathcal{F}}}^{\text{RB}} \leftarrow []$ 
19:  end for
20:  for  $i := 1$  to  $n_\omega$  do
21:     $[u^{h, \text{M}' \cdot \text{N}}(\cdot; \mu_{+i}^{\text{test}}), \sim, \sim] \leftarrow \text{PR-RBC-1st-step-reduction-Online}(\sim, \mu^{\text{test}}, \omega_i)$ 
22:     $\underline{\underline{u}}_g : u^{h, \text{M}' \cdot \text{N}}(\cdot; \mu_{+i}^{\text{test}}) = \sum_{j=1}^{\mathcal{N}^h} (\underline{\underline{u}}_g)_j \varphi_j$ 
23:     $\underline{\underline{Z}}(:, i) \leftarrow \underline{\underline{u}}_g(I(:))$ 
24:     $\underline{\underline{r}}_0(i) \leftarrow \underline{\underline{Z}}(:, i)^\dagger \times \underline{\underline{X}}^{h, \text{norm}}(I(:), I(:)) \times \underline{\underline{Z}}(:, i)$ 
25:  end for
26:  while  $i < N$  and  $i < n_\omega - 1$  and  $\underline{\underline{e}}(i+1) > \epsilon$  do
27:     $I_g \leftarrow [I_g \ i_g]$ 
28:     $i \leftarrow i + 1$ 
29:     $\underline{\underline{u}}_g \leftarrow \underline{\underline{Z}}(:, i_g)$ 
30:    if  $\underline{\underline{X}}^{\text{RB}} \neq []$  then
31:       $\underline{\underline{u}}_g \leftarrow \underline{\underline{u}}_g - \underline{\underline{X}}^{\text{RB}} \times (\underline{\underline{X}}^{\text{RB}})^\dagger \times \underline{\underline{X}}^{h, \text{norm}}(I(:), I(:)) \times \underline{\underline{u}}_g$ 
32:    end if
33:     $\underline{\underline{u}}_g \leftarrow \frac{\underline{\underline{u}}_g}{\sqrt{\underline{\underline{u}}_g^\dagger \times \underline{\underline{X}}^{h, \text{norm}}(I(:), I(:)) \times \underline{\underline{u}}_g}}$ 
34:     $\underline{\underline{X}}^{\text{RB}} \leftarrow [\underline{\underline{X}}^{\text{RB}} \ \underline{\underline{u}}_g]$ 

```

```

35:  $\underline{\underline{\mathcal{B}}}^{\text{new}} \leftarrow (\underline{\underline{\mathcal{X}}}^{\text{RB}})^{\dagger} \times (\underline{\underline{\mathcal{X}}}^{h,\text{norm}}(I(:), I(:)) \times \underline{\underline{\mathcal{X}}}^{\text{RB}}(:, i))$ 
36:  $\underline{\underline{\mathcal{B}}}^{\text{RB}} \leftarrow \begin{bmatrix} \underline{\underline{\mathcal{B}}}^{\text{RB}} & \underline{\underline{\mathcal{B}}}^{\text{new}}(1 : i - 1) \\ \underline{\underline{\mathcal{B}}}^{\text{new}}(1 : i - 1)^{\dagger} & \underline{\underline{\mathcal{B}}}^{\text{new}}(i) \end{bmatrix}$ 
37:  $\underline{\underline{\mathcal{D}}}^{\text{RB}} \leftarrow [\underline{\underline{\mathcal{D}}}^{\text{RB}} \quad \underline{\underline{\mathcal{Z}}}^{\dagger} \times (\underline{\underline{\mathcal{X}}}^{h,\text{norm}}(I(:), I(:)) \times \underline{\underline{\mathcal{X}}}^{\text{RB}}(:, i))]$ 
38: for  $r := 1$  to  $Q^{a+}$  do
39:  $\underline{\underline{\mathcal{A}}}^{\text{new}} \leftarrow (\underline{\underline{\mathcal{X}}}^{\text{RB}})^{\dagger} \times \underline{\underline{\mathcal{A}}}^h_r(I(:), I(:)) \times \underline{\underline{\mathcal{X}}}^{\text{RB}}(:, i)$ 
40:  $\underline{\underline{\mathcal{A}}}^{\text{RB}}_r \leftarrow \begin{bmatrix} \underline{\underline{\mathcal{A}}}^{\text{RB}}_r & \underline{\underline{\mathcal{A}}}^{\text{new}}(1 : i - 1) \\ \underline{\underline{\mathcal{A}}}^{\text{new}}(1 : i - 1)^{\dagger} & \underline{\underline{\mathcal{A}}}^{\text{new}}(i) \end{bmatrix}$ 
41: end for
42: for  $r := 1$  to  $Q^{f+}$  do
43:  $\underline{\underline{\mathcal{F}}}^{\text{RB}}_r \leftarrow \begin{bmatrix} \underline{\underline{\mathcal{F}}}^{\text{RB}}_r & \underline{\underline{\mathcal{F}}}^{\text{RB}}_r \\ \underline{\underline{\mathcal{X}}}^{\text{RB}}(:, i)^{\dagger} \times \underline{\underline{\mathcal{F}}}^h_r(I(:)) \end{bmatrix}$ 
44: end for
45: for  $r := 1$  to  $n_{\omega}$  do
46:  $\underline{\underline{\mathcal{A}}}^{\text{RB}}(\mu_{+j}^{\text{test}}) \leftarrow \sum_{r=1}^{Q^{a+}} \Theta_k^{a+}(\mu_{+j}^{\text{test}}) \underline{\underline{\mathcal{A}}}^{\text{RB}}_r$ 
47:  $\underline{\underline{\mathcal{F}}}^{\text{RB}}(\mu_{+j}^{\text{test}}) \leftarrow \sum_{r=1}^{Q^{f+}} \Theta_k^{f+}(\mu_{+j}^{\text{test}}) \underline{\underline{\mathcal{F}}}^{\text{RB}}_r$ 
48:  $\underline{\underline{\mathcal{U}}}^{\text{RB}}(\mu_{+j}^{\text{test}}) \leftarrow (\underline{\underline{\mathcal{A}}}^{\text{RB}}(\mu_{+j}^{\text{test}}))^{-1} \times \underline{\underline{\mathcal{F}}}^{\text{RB}}(\mu_{+j}^{\text{test}})$ 
49:  $r^{\text{add}} \leftarrow \underline{\underline{\mathcal{D}}}^{\text{RB}}(r, :) \times \underline{\underline{\mathcal{U}}}^{\text{RB}}(\mu_{+j}^{\text{test}})$ 
50:  $\underline{\underline{r}}(j) \leftarrow \underline{\underline{r}}_0(j) - r^{\text{add}} - (r^{\text{add}})^{\dagger} + (\underline{\underline{\mathcal{U}}}^{\text{RB}}(\mu_{+j}^{\text{test}}))^{\dagger} \times \underline{\underline{\mathcal{B}}}^{\text{RB}} \times \underline{\underline{\mathcal{U}}}^{\text{RB}}(\mu_{+j}^{\text{test}})$ 
51: end for
52:  $[R_i, i_g] = \max(\underline{\underline{r}})$ 
53:  $\underline{\underline{e}}(i + 1) \leftarrow R_i / R_1$ 
54: end while
55:  $\underline{\underline{e}} \leftarrow \underline{\underline{e}}(2 : i + 1)$ 
56: return  $\underline{\underline{\mathcal{X}}}^{\text{RB}}, \underline{\underline{e}}, I_g$ 
57: end function

```

Algorithm 2 PR-RBC-Two-Step-Reduction algorithm

```

1: function PR-RBC-TWO-STEP-REDUCTION( $\mu^{\text{test}}, \Xi_\omega, n_\omega, Q^{a+}, Q^{f+}, \epsilon, N, \underline{\underline{X}}^{h,\text{norm}}, \mathcal{I}, \mathcal{N}^h, \{\Theta_r^{a+}(\cdot), 1 \leq r \leq Q^{a+}\},$ 
    $\{\Theta_r^{f+}(\cdot), 1 \leq r \leq Q^{f+}\}, \{\underline{\underline{\mathcal{A}}}_r^h, 1 \leq r \leq Q^{a+}\}, \{\underline{\underline{\mathcal{F}}}_r^h, 1 \leq r \leq Q^{f+}\}, \{\varphi_j, 1 \leq j \leq \mathcal{N}^h\}, \{\Theta_r^m(\cdot), 1 \leq r \leq Q^m\},$ 
    $\{\Theta_r^c(\cdot), 1 \leq r \leq Q^c\}, \{\Theta_r^a(\cdot), 1 \leq r \leq Q^a\}, \{\Theta_r^f(\cdot), 1 \leq r \leq Q^f\}, \{\underline{\underline{M}}_r^{th}, 1 \leq r \leq Q^m\}, \{\underline{\underline{C}}_r^{th}, 1 \leq r \leq Q^c\},$ 
    $\{\underline{\underline{\mathcal{A}}}_r^{th}, 1 \leq r \leq Q^a\}, \{\underline{\underline{\mathcal{F}}}_r^{th}, 1 \leq r \leq Q^f\}, \Delta t, N_t, \gamma_t, \beta_t, \underline{\underline{u}}_0^h, \underline{\underline{\dot{u}}}_0^h)$ 
2:  $\underline{\underline{X}}^{\text{RB}} \leftarrow \text{SG} - 2\text{nd} - \text{step} - \text{reduction}(\mu^{\text{test}}, \Xi_\omega, n_\omega, \mathcal{N}^h,$ 
    $\underline{\underline{X}}^{h,\text{norm}}, \mathcal{I}, \epsilon, N, \{\varphi_j, 1 \leq j \leq \mathcal{N}^h\}, Q^{a+}, Q^{f+}, \{\Theta_r^{a+}(\cdot), 1 \leq r \leq Q^{a+}\},$ 
    $\{\Theta_r^{f+}(\cdot), 1 \leq r \leq Q^{f+}\}, \{\underline{\underline{\mathcal{A}}}_r^h, 1 \leq r \leq Q^{a+}\}, \{\underline{\underline{\mathcal{F}}}_r^h, 1 \leq r \leq Q^{f+}\})$ 
3:  $\underline{\underline{M}}_{\mu^{\text{test}}}^{th} \leftarrow \sum_{r=1}^{Q^m} \Theta_r^m(\mu^{\text{test}}) \underline{\underline{M}}_r^{th}$ 
4:  $\underline{\underline{C}}_{\mu^{\text{test}}}^{th} \leftarrow \sum_{r=1}^{Q^c} \Theta_r^c(\mu^{\text{test}}) \underline{\underline{C}}_r^{th}$ 
5:  $\underline{\underline{\mathcal{A}}}_{\mu^{\text{test}}}^{th} \leftarrow \sum_{r=1}^{Q^a} \Theta_r^a(\mu^{\text{test}}) \underline{\underline{\mathcal{A}}}_r^{th}$ 
6:  $\underline{\underline{\mathcal{F}}}_{\mu^{\text{test}}}^{th} \leftarrow \sum_{r=1}^{Q^f} \Theta_r^f(\mu^{\text{test}}) \underline{\underline{\mathcal{F}}}_r^{th}$ 
7:  $\underline{\underline{M}}_{\mu^{\text{test}}}^{\text{tRB}} \leftarrow (\underline{\underline{X}}^{\text{RB}})^\dagger \times \underline{\underline{M}}_{\mu^{\text{test}}}^{th} (I(\cdot), I(\cdot)) \times \underline{\underline{X}}^{\text{RB}}$ 
8:  $\underline{\underline{C}}_{\mu^{\text{test}}}^{\text{tRB}} \leftarrow (\underline{\underline{X}}^{\text{RB}})^\dagger \times \underline{\underline{C}}_{\mu^{\text{test}}}^{th} (I(\cdot), I(\cdot)) \times \underline{\underline{X}}^{\text{RB}}$ 
9:  $\underline{\underline{\mathcal{A}}}_{\mu^{\text{test}}}^{\text{tRB}} \leftarrow (\underline{\underline{X}}^{\text{RB}})^\dagger \times \underline{\underline{\mathcal{A}}}_{\mu^{\text{test}}}^{th} (I(\cdot), I(\cdot)) \times \underline{\underline{X}}^{\text{RB}}$ 
10:  $\underline{\underline{\mathcal{F}}}_{\mu^{\text{test}}}^{\text{tRB}} \leftarrow (\underline{\underline{X}}^{\text{RB}})^\dagger \times \underline{\underline{\mathcal{F}}}_{\mu^{\text{test}}}^{th} (I(\cdot))$ 
11:  $\underline{\underline{\mathcal{T}}}_{\mu^{\text{test}}}^{\text{RB}} \leftarrow \underline{\underline{M}}_{\mu^{\text{test}}}^{\text{tRB}} + \Delta t \times \gamma_t \times \underline{\underline{C}}_{\mu^{\text{test}}}^{\text{RB}} + \Delta t^2 \times \beta_t \times \underline{\underline{\mathcal{A}}}_{\mu^{\text{test}}}^{\text{RB}}$ 
12:  $\underline{\underline{u}}_0^{\text{RB}} \leftarrow (\underline{\underline{X}}^{\text{RB}})^\dagger \times \underline{\underline{u}}_0^h$ 
13:  $\underline{\underline{\dot{u}}}_0^{\text{RB}} \leftarrow (\underline{\underline{X}}^{\text{RB}})^\dagger \times \underline{\underline{\dot{u}}}_0^h$ 
14:  $\underline{\underline{\mathcal{F}}}_{\mu^{\text{test}}}^{\text{tRB}} \leftarrow -\underline{\underline{C}}_{\mu^{\text{test}}}^{\text{RB}} \times \underline{\underline{\dot{u}}}_0^{\text{RB}} - \underline{\underline{\mathcal{A}}}_{\mu^{\text{test}}}^{\text{RB}} \times \underline{\underline{u}}_0^{\text{RB}}$ 
15:  $\underline{\underline{\dot{u}}}_0^{\text{RB}} \leftarrow (\underline{\underline{M}}_{\mu^{\text{test}}}^{\text{RB}})^{-1} \times \underline{\underline{\mathcal{F}}}_{\mu^{\text{test}}}^{\text{tRB}}$ 
16: for  $j := 1$  to  $N_t$  do
17:    $t_j \leftarrow j \times \Delta t$ 
18:    $\underline{\underline{\mathcal{F}}}_{\mu^{\text{test}}}^{\text{tRB}} \leftarrow -\underline{\underline{C}}_{\mu^{\text{test}}}^{\text{RB}} \times (\underline{\underline{\dot{u}}}_{j-1}^{\text{RB}} + \Delta t(1 - \gamma_t)\underline{\underline{\ddot{u}}}_{j-1}^{\text{RB}}) - \underline{\underline{\mathcal{A}}}_{\mu^{\text{test}}}^{\text{RB}} \times (\underline{\underline{u}}_{j-1}^{\text{RB}} + \Delta t\underline{\underline{\dot{u}}}_{j-1}^{\text{RB}} + \Delta t^2(1 - \beta_t)\underline{\underline{\ddot{u}}}_{j-1}^{\text{RB}})$ 
19:    $\underline{\underline{\ddot{u}}}_j^{\text{RB}} \leftarrow (\underline{\underline{\mathcal{T}}}_{\mu^{\text{test}}}^{\text{RB}})^{-1} \times [\underline{\underline{\mathcal{F}}}_{\mu^{\text{test}}}^{\text{t}}(t_j, \mu^{\text{test}}) \times \underline{\underline{\mathcal{F}}}_{\mu^{\text{test}}}^{\text{RB}} + \underline{\underline{\mathcal{F}}}_{\mu^{\text{test}}}^{\text{tRB}}]$ 
20:    $\underline{\underline{u}}_j^{\text{RB}} \leftarrow \underline{\underline{u}}_{j-1}^{\text{RB}} + \Delta t\underline{\underline{\dot{u}}}_{j-1}^{\text{RB}} + \Delta t^2[(\frac{1}{2} - \beta_t)\underline{\underline{\ddot{u}}}_{j-1}^{\text{RB}} + \beta_t\underline{\underline{\ddot{u}}}_j^{\text{RB}}]$ 
21:    $\underline{\underline{\dot{u}}}_j^{\text{RB}} \leftarrow \underline{\underline{\dot{u}}}_{j-1}^{\text{RB}} + \Delta t[(1 - \gamma_t)\underline{\underline{\ddot{u}}}_{j-1}^{\text{RB}} + \gamma_t\underline{\underline{\ddot{u}}}_j^{\text{RB}}]$ 
22: end for
23: return  $\{\underline{\underline{u}}_j^{\text{RB}}(\mu^{\text{test}})\}_{1 \leq j \leq N_t}$ 
24: end function

```

References

References

- [1] M. Meyer, H. G. Matthies, Efficient model reduction in non-linear dynamics using the karhunen-loève expansion and dual-weighted-residual methods, *Computational Mechanics* 31 (1-2) (2003) 179–191.
- [2] K. Kunisch, S. Volkwein, Galerkin proper orthogonal decomposition methods for parabolic problem, *Numerische Mathematik* 90 (2001) 117–148.
- [3] K. Kunisch, S. Volkwein, Galerkin proper orthogonal decomposition methods for a general equation in fluid dynamics, *SIAM Journal on Numerical Analysis* 40 (2) (2003) 492–515.
- [4] M. Rathinam, L. R. Petzold, A new look at proper orthogonal decomposition, *SIAM Journal on Numerical Analysis* 41 (5) (2003) 1893–1925.
- [5] M. A. Grepl, Y. Maday, N. C. Nguyen, A. T. Patera, Efficient reduced-basis treatment of nonaffine and nonlinear partial differential equations, *ESAIM Mathematical Modelling and Numerical Analysis* 41 (3) (2007) 575–605.
- [6] M. A. Grepl, A. T. Patera, A posteriori error bounds for reduced-basis approximations of parametrized parabolic partial differential equations, *ESAIM Mathematical Modelling and Numerical Analysis* 39 (1) (2005) 157–181.
- [7] M. A. Grepl, Certified Reduced Basis Methods for Nonaffine Linear Time-Varying and Nonlinear Parabolic Partial Differential Equations, *Mathematical Models and Methods in Applied Sciences* 22 (3), paper 1150015.
- [8] H. Haasdonk, M. Ohlberger, Reduced basis method for finite volume approximations of parametrized linear evolution equations, *ESAIM Mathematical Modelling and Numerical Analysis* 42 (2008) 277–302.
- [9] A. Tan, Reduced Basis Methods for 2nd Order Wave Equation: Application to One Dimensional Seismic Problem, masters Thesis, Singapore-MIT Alliance, National University of Singapore (2006).
- [10] D. Huynh, D. Knezevic, A. Patera, A static condensation reduced basis element method: Approximation and a posteriori error estimation, *ESAIM Mathematical Modelling and Numerical Analysis* 47 (1) (2013) 213–251.
- [11] J. L. Eftang, A. Patera, Port Reduction in Component-Based Static Condensation for Parametrized Problems: Approximation and a Posteriori Error Estimation, *International Journal for Numerical Methods in Engineering* 96 (5) (2013) 269–302.
- [12] K. Smetana, A new certification framework for the port reduced static condensation reduced basis element method, *Computer Methods in Applied Mechanics and Engineering* 283 (2015) 352–383.
- [13] K. Smetana, A. T. Patera, Optimal local approximation spaces for component-based static condensation procedures, *SIAM Journal on Scientific Computing* 38 (5) (2016) A3318–A3356.
- [14] A. C. Antoulas, C. A. Beattie, S. Gugercin, Interpolatory Model Reduction of Large-Scale Dynamical Systems, in: J. Mohammadpour, K. Grigoriadis (Eds.), *Efficient Modeling and Control of Large-Scale Systems*, Springer, Boston, MA, 2010, pp. 3–58.
- [15] C. Beattie, S. Gugercin, Model Reduction by Rational Interpolation, arXiv:1409.2140v1 [math.NA] (2014).
- [16] D. Huynh, D. Knezevic, A. Patera, A laplace transform certified reduced basis method; application to the heat equation and wave equation, *C. R. Acad. Sci. Paris Series I* 349 (7-8) (2011) 401–405.
- [17] J. L. Eftang, D. Huynh, D. Knezevic, A. Patera, A Two-Step Certified Reduced Basis Method, *Journal of Scientific Computing* 51 (1) (2012) 28–58.
- [18] A. T. Patera, M. Yano, An lp empirical quadrature procedure for parametrized functions, *Comptes Rendus Mathématique* 355.
- [19] M. Barrault, Y. Maday, N. C. Nguyen, A. Patera, An empirical interpolation method: Application to efficient reduced-basis discretization of partial differential equations, *C. R. Acad. Sci. Paris Series I* 339 (9) (2004) 667–672.
- [20] D. Huynh, D. Knezevic, A. Patera, A static condensation reduced basis element method: Complex problems, *Computer Methods in Applied Mechanics and Engineering* 259 (2013) 197–216.
- [21] R. Craig, M. Bampton, Coupling of Substructures for Dynamic Analyses, *AIAA Journal* 3 (4) (1968) 678–685.
- [22] W. C. Hurty, Dynamic analysis of structural systems using component modes, *AIAA Journal* 3 (4) (1965) 678–684.
- [23] U. Hetmaniuk, R. Lehoucq, A special finite element method based on component mode synthesis, *ESAIM Mathematical Modelling and Numerical Analysis* 44 (3) (2010) 401–421.
- [24] A. K. Noor, J. M. Peters, Reduced basis technique for nonlinear analysis of structures, *AIAA Journal* 18 (4) (1980) 455–462.
- [25] B. O. Almroth, P. Stern, F. A. Brogan, Automatic Choice of Global Shape Functions in Structural Analysis, *AIAA Journal* 16 (5) (1978) 525–528.
- [26] G. Rozza, D. B. P. Huynh, A. T. Patera, Reduced basis approximation and a posteriori error estimation for affinely parametrized elliptic coercive partial differential equations, *Archives of Computational Methods in Engineering* 15 (3) (2008) 229–275.
- [27] Y. Maday, E. M. Rønquist, The reduced basis element method: Application to a thermal fin problem, *SIAM Journal on Scientific Computing* 26 (1) (2004) 240–258.
- [28] E. L. Wilson, The static condensation algorithm, *International Journal for Numerical Methods in Engineering* 8 (1) (1974) 198–203.
- [29] K. Veroy, C. Prud’homme, D. V. Rovas, A. T. Patera, A posteriori error bounds for reduced-basis approximation of parametrized noncoercive and nonlinear elliptic partial differential equations, in: *Proceedings of the 16th AIAA Computational Fluid Dynamics Conference*, AIAA, Orlando, FL, 2003, pp. 1–18.
- [30] J. L. Eftang, A. Patera, A port-reduced static condensation reduced basis element method for large component-synthesized structures: approximation and a posteriori error estimation, *Advanced Modeling and Simulation in Engineering Sciences* 1 (1) (2014) 3.
- [31] F. Chiba, T. Kako, Stability and error analyses by energy estimate for Newmark’s method, Tech. Rep. NIFS-PROC-40, National Inst. for Fusion Science, Nagoya, Japan (1999).
- [32] R. Nickell, On the Stability of Approximation Operators in Problems of Structural Dynamics, *International Journal of Solids and Structures* 7 (3) (1971) 301–319.
- [33] M. Q. Feng, S. C. Lee, Determining the effective system damping of highway bridges, Tech. Rep. CA-UCI-2009-001, California Department of Transportation, Sacramento, CA (2009).

- [34] M. Musiał, J. Grosel, Determining the young's modulus of concrete by measuring the eigenfrequencies of concrete and reinforced concrete beams, *Construction and Building Materials*, Elsevier 121 (2016) 44–52.
- [35] M. Yu, G. Wu, L. Kong, Y. Tang, Tire-Pavement Friction Characteristics with Elastic Properties of Asphalt Pavements, *Applied Sciences* 7 (2017) 1123.
- [36] P. Yap, Truck tire types and road contact pressures, in: *Proceedings of the 2nd International Symposium on Heavy Vehicle Weights and Dimensions*, The Roads and Transport Association of Canada, Canada, 1989.
- [37] M. P. Culmo, Connection Details for Prefabricated Bridge Elements and Systems, Tech. Rep. FHWA-IF-09-010, Federal Highway Administration, Washington, DC (2009).
- [38] F. Barth, J. R. Frosch, M. Abou-Zeid, H. J. Allen, J. P. Barlow, M. E. Brander, K. Carlson, D. Darwin, F. H. Fouad, D. W. Fowler, G. T. Halvorsen, W. Hansen, M. N. Hassoun, H. Haynes, P. Hedli, T. C. Liu, E. G. Nawy, R. W. Poston, R. J. Rhoads, A. Scanlon, E. K. Schrader, W. Suaris, Z. A. Zielinski, Control of Cracking of Concrete Structures, Tech. Rep. ACI 224R-01, American Concrete Institute, Farmington Hills, MI (2001).
- [39] S. S. G. Balakumaran, R. E. Weyers, M. C. Brown, Linear Cracking in Bridge Decks, Tech. Rep. FHWA/VTRC 18-R13, Virginia Transportation Research Council, Charlottesville, VA (2018).
- [40] A. Logan, W. Choi, A. Mirmiran, S. Rizkalla, P. Zia, Short-Term Mechanical Properties of High-Strength Concrete, *ACI Materials Journal* 106 (2009) 413–418.
- [41] D. Xiao, F. Fang, C. C. Pain, I. M. Navon, Domain decomposition non-intrusive reduced order modelling of non-linear flow dynamics, *Computer Methods in Applied Mechanics and Engineering* 354.
- [42] MATLAB, Version 9.4 (r2018a), the MathWorks Inc., Natick, Massachusetts (2015).